Industrial Crops & Products 235 (2025) 121749

Contents lists available at ScienceDirect

Industrial Crops & Products

journal homepage: www.elsevier.com/locate/indcrop

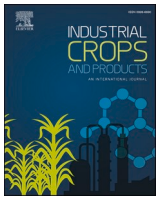

Effects of methyl jasmonate and chitosan nanoparticle treatments on field-grown hemp inflorescences: Integrating transcriptomic and secondary metabolite insights

Giulio Testone [a,1], Roméo Arago Douguè Kentsop [b,1], Donato Giannino [a], Cassia da Silva Linge [b,2], Incoronata Galasso [b], Annamaria Genga [b], Andrea Delledonne [b], Stefano Biffani [b], Gabriella Roda [d], Giovanna Frugis [c,*], Monica Mattana [b,*]

[a] Institute for Biological Systems, National Research Council (CNR), Area territoriale di Ricerca di Roma 1, Strada Provinciale 35D, n. 9, Rome, Montelibretti 00010, Italy
[b] Institute of Agricultural Biology and Biotechnology, National Research Council (CNR), Via Alfonso Corti 12, Milan 20133, Italy
[c] Institute of Agricultural Biology and Biotechnology, National Research Council (CNR), Area territoriale di Ricerca di Roma 1, Strada Provinciale 35D, n. 9, Rome, Montelibretti 00010, Italy
[d] Department of Pharmaceutical Sciences, University of Milan, Via Trentacoste, 2, Milan 20134, Italy

ARTICLE INFO

Keywords:
Cannabis sativa
Elicitation
Methyl jasmonate
Chitosan nanoparticles
Phenolics
Cannabinoids
WGCNA

ABSTRACT

Industrial hemp (*Cannabis sativa* L.) is valued for its industrial, food, medical and recreational applications due to its bioactive secondary metabolites, including phenols, cannabinoids and terpenes, which accumulate at low concentrations (<1 % dry weight) in female inflorescences and increase under stress. This study aimed to enhance these compounds by applying methyl jasmonate (MeJA), either alone or encapsulated in chitosan nanoparticles, to female plants of the dioecious cultivar Tiborszallasi grown under field conditions. Treatments included 1 mM and 10 mM MeJA, chitosan nanoparticles (CHT) alone and nanoparticles loaded with 1 mM MeJA. Inflorescences were sampled at early and mature developmental stages, at two time-points per stage: 6 h and 6 days post-treatment. Overall, treatment with 10 mM MeJA significantly increased phenols (+21.2 %), flavonoids (+49.5 %), antioxidant activity (+43.7 %), CBDA (+78.4 %) and terpenes (+94.7 %) in mature inflorescences harvested 6 days after treatment. RNA-Seq analysis scored MeJA marker responses and revealed dose-dependent transcriptional changes. Weighted correlation network and gene co-expression network analyses revealed key regulatory and metabolic genes associated with secondary metabolism, including cannabinoid, phenylpropanoid and terpene pathways. These analyses underscored the central role of the fatty acid biosynthetic pathway in cannabinoid accumulation and highlighted a TALE- and SQUAMOSA-driven transcriptional network as pivotal in the developmental transition from meristem-rich to highly differentiated inflorescences specialized in secondary metabolite production. Overall, this study provides insights into MeJA elicitation of secondary metabolism and identifies regulatory hubs and candidates not previously associated with secondary metabolism in *Cannabis sativa* for enhancing the therapeutic and commercial potential of industrial hemp.

1. Introduction

Industrial hemp (*Cannabis sativa* L., Fam. *Cannabaceae*) is a versatile crop used in food, textile, pharmaceutical, and bioenergy industries. It is considered sustainable due to its fast growth, environmental adaptability, and low input requirements (Amaducci et al., 2015). Traditionally, hemp has been cultivated for its bast fibers (used in textiles and ropes) and nutrient-rich seeds containing essential fatty acids and proteins. Additionally, hemp has long attracted attention for its high content of bioactive metabolites and has been used for medical purposes

* Corresponding authors.
E-mail addresses: giovanna.frugis@cnr.it (G. Frugis), monica.mattana@cnr.it (M. Mattana).
[1] These authors contributed equally to this work.
[2] Present address: Department of Agricultural and Environmental Sciences - Production, Landscape, Agroenergy, University of Milan, Via Celoria 2 - 20133 Milan, Italy

https://doi.org/10.1016/j.indcrop.2025.121749
Received 17 April 2025; Received in revised form 11 July 2025; Accepted 14 August 2025
Available online 20 August 2025
0926-6690/© 2025 The Author(s). Published by Elsevier B.V. This is an open access article under the CC BY license (http://creativecommons.org/licenses/by/4.0/).

for over 2700 years, with evidence from northwestern China (Russo et al., 2008).

The two main classes of *Cannabis*-derived metabolites are cannabinoids and terpenes, though flavonoids, phenolic acids, lignans, and alkaloids have been also identified (Lowe et al., 2021). Based on Δ^9-tetrahydrocannabinolic and cannabidiolic acids ratio (THCA/CBDA), three main chemotypes are distinguished: chemotype I (drug- or medical-type plants) with a high ratio (>>1.0); chemotype II with an intermediate ratio (0.5 −2.0), and chemotype III (industrial or fiber-type plants) with a low (<<1.0) ratio (Aizpurua-Olaizola et al., 2016). Moreover, cannabidiol (CBD) and Δ^9-tetrahydrocannabinol (THC) are renowned for their anti-inflammatory, analgesic, and neuroprotective activities. As for phenolic compounds, flavonoids and phenolic acids exhibit antioxidant activity, contributing to plant defence mechanisms and human health benefits (Andre et al., 2016).

Unlike other drug-producing plants whose growth is restricted to small geographical areas, *Cannabis* is distributed worldwide across diverse climates (Amaducci et al., 2015). However, bioactive compounds levels vary based on growing conditions, soil type, latitude, genotype and harvest time. The main metabolites accumulate in glandular trichomes which mostly coat the female inflorescences (Livingston et al., 2020). Since secondary metabolites are synthesized at low concentrations and are induced under stress conditions, optimizing growth parameters and using strategies to enhance secondary metabolism are key factors for boosting bioactive compound production (Trono, 2024).

Elicitation is a widely recognized strategy to stimulate bioactive compound biosynthesis in medicinal and aromatic species, both *in vitro* and in whole plants (Thakur et al., 2019). Salicylic acid and jasmonates are plant signaling compounds induced by pathogen attack and wounding that trigger plant defense responses. These molecules have been used as elicitors in several plant species, including medical and industrial hemp (Garrido et al., 2022; Welling et al., 2023). Specifically, methyl jasmonate (MeJA), has been adopted to elicit secondary metabolite production in both *in vitro* hemp cultures and whole plants (Gabotti et al., 2019; Garrido et al., 2022; Welling et al., 2023). However, the effectiveness of MeJA treatments varied depending on multiple factors, including plant system (*in vitro vs*. whole plant), genotype/chemotype (drug *vs*. industrial hemp), elicitor concentration, harvest time and inflorescence developmental stage (Trono, 2024). Recently, nanoparticles have emerged as effective elicitors of specialized metabolites (Mmereke et al., 2024). Interest in nanotechnology is increasing in the field of precision farming, where it is being applied to crop management through targeted delivery of nutrients and plant protection agents (Duhan et al., 2017). In recent years, several studies have highlighted that nanoparticles affect the biosynthesis of secondary metabolites in plant and culture systems (Martínez-Chávez et al., 2024). Most of the nanoparticles developed are of metallic origin, raising issues related to cytotoxicity and possible constraints on the subsequent use of the produced metabolites (Humbal and Pathak, 2023). To overcome this problem, biopolymeric nanoparticles, formulated with chitosan, have been used as elicitors (Humbal and Pathak, 2023). Namely, chitosan-based nanoparticles have been shown to successfully enhance phenolic content as well as phenylalanine ammonia-lyase (PAL) and antioxidant enzyme activities (Mmereke et al., 2024). Their effectiveness can be further improved by loading them with active ingredients, allowing gradual release while reducing volatilization and run-off (Picchi et al., 2022). However, up to now, most of the studies have been conducted on *in vitro* cultures and much less has been performed on field growing plants (Arya et al., 2022). In recent years, the global industrial hemp market has experienced impressive growth. Valued at USD 7.12 billion in 2024, it is projected to reach USD 8.6 billion by 2025, with a compound annual growth rate (CAGR) of 20.8 % (The Business Research Company, 2024). A key driver of this expansion is the hemp-derived cannabidiol (CBD) segment, which alone is expected to grow to USD 46.25 billion by 2034, at a CAGR of 16.93 % (GlobeNewswire, 2025). This surge reflects rising consumer demand for natural and sustainable products, as well as increasing interest in the therapeutic potential of hemp metabolites. In this context, implementing strategies that enhance the biosynthesis of secondary metabolites, and understanding the genetic mechanisms behind their production, is essential for maximizing yields of bioactive compounds and ensuring the sustainable development of the hemp sector in an increasingly dynamic global market.

Recent advances in molecular resources have provided valuable insights into hemp's genetic and metabolic pathways (Pancaldi et al., 2025). Multi-omics approaches have gained traction (Sirangelo et al., 2022), including studies on methyl jasmonate (MeJA) treatments (Apicella et al., 2022). However, much of this research has so far been conducted under controlled conditions, highlighting the need for further investigations in field-relevant contexts. Moreover, despite recent advances, data integration remains a significant challenge, underscoring the need for robust, Cannabis-specific bioinformatics tools to enable seamless analysis and interpretation, and to support the optimization of cultivation technologies. Thus, considering that the application of elicitation techniques in open-field cultivated hemp remains insufficiently explored, our study aims to address this gap by applying specific elicitation strategies to hemp inflorescences, analyzing the transcriptional responses involved in secondary metabolite accumulation, and highlighting hub genes responsible for this enhancement. Specifically, in this open field study we investigated the effects of MeJA and chitosan nanoparticles, applied either alone or in combination with MeJA, on female Tiborszallasi hemp inflorescences with the aim to develop agronomic strategies to modulate key compounds (cannabinoids, phenolics, and terpenes) levels and yield-related properties (e.g., antioxidant activity). Additionally, we investigated the molecular mechanisms underlying inflorescence responses to various treatments across developmental stages. These findings provide new insights into the regulation of key metabolic pathways and identify potential molecular targets for improving the phytochemical profile of industrial hemp.

2. Materials and methods

2.1. Plant materials and treatments

Seeds of the dioecious *Cannabis sativa*, Tiborszallasi, were germinated in trays. At the stage of the first leaf, DNA was extracted, and PCR analysis was performed according to Mandolino et al. (1999) for sex determination. Only female plants were transplanted in the field (April 26, 2022) and grown until complete inflorescences maturation.

The experimental field was established at "Orto Botanico" of the University of Milan (45°29'2.76"N, 9°14'3.48"E, 122 m a.s.l). A randomized block design was adopted to compare five treatments from three biological replicates as described below. The area of each parcel was 6 m^2 and contained 50 plants. An analysis of the soil texture and macronutrients was performed, identifying the soil type as silty loam (Table S1). The meteorological data were provided by the ARPA Lombardia weather station in Milan, Lambrate (available upon request).

Elicitation treatments were performed with chitosan nanoparticles (CHT), CHT charged with 1 mM MeJA 1 mM MeJA and 10 mM MeJA. MeJA 95 %, was dissolved in 1 % ethanol and 0.1 % Tween 20. Chitosan nanoparticles were prepared following the method reported by Picchi et al. (2022). Encapsulation efficiency of MeJA into the nanoparticles was assessed using a previously published method (Arya et al., 2022). The MeJA was extracted from the nanoparticles using a 0.1 M hydrochloric acid solution, and its content was quantified via UV–VIS spectroscopy by measuring the absorbance at 285 nm and the Encapsulation Efficiency (EE) was calculated using the following equation:

$$EE\ (\%) = (\text{Free MeJA in supernatant}) / (\text{Total MeJA added}) \times 100$$

An EE of 76 ± 4 % was achieved, in line with the results reported by Arya et al. (2022).

Treatments were applied as foliar spray to the point of runoff, starting at the beginning of the flowering period, applied three times, once per week, until the first harvest (DS1, early developmental stage, Fig. 1A). Then, three more applications were dispensed, once per week, until the second harvest (DS2, mature developmental stage, Fig. 1B). DS1 corresponded to the phenological growth stage 63 of the BBCH scale of flowering (30 % of flowers opened), whereas DS2 corresponded to the 65/67 of the BBCH scale that means full flowering (Mishchenko et al., 2017).

Inflorescences were collected in triplicate, and at each DS, samples were taken 6 h and 6 days after treatments, corresponding to HT1 and HT2, respectively.

The top 30 cm of inflorescences were taken, frozen and ground in liquid nitrogen. Part of the powder was stored at –80°C for RNA extraction, while the rest was freeze-dried for biochemical analysis.

2.2. Extraction and metabolite analyses

2.2.1. Total phenols, total flavonoids and antioxidant activity

A total of 20 mg of dry material was extracted with 1.5 mL of ethanol 80 % followed by vortexing, sonication for 30 min, and shaken overnight at RT. After centrifugation at 16.000 rcf for 10 min the supernatant was diluted 1:5 before use. The TPC and AA (DPPH assay) were determined following Gabotti et al. (2019). The TFC was measured according to Pękal and Pyrzynska (2014) using catechin as standard (Merck, Germany).

2.2.2. Cannabinoid analyses

The extraction and HPLC analysis were performed following Dei Cas et al. (2020) with modification. Briefly, 50 mg of dry inflorescences were suspended in 5 mL of ethanol, vortexed for 3 min, centrifuged for 10 min at 16.000 rcf, and the supernatant was diluted 1:10 with the solvents of the initial HPLC phase. The analytical system consisted of a *JASCO* HPLC-DAD (Jasco, Japan). The separation column was a reversed-phase Shimadzu NexLeaf CBX for Potency, 2.7 µm (150 mm×4.6 mm), protected by an Ascentis Express 90 Å C18 guard column 2.7 µm (0.5 cm×3.0 mm). The gradient was between eluent A (water) and eluent B (acetonitrile) both containing 0.085 % phosphoric acid. The elution gradient was the following: 0–3 (70 % B), 3–7 min (70–85 % B), 7.0–7.1 min (85–95 % B), 7.1–8.0 min (95 % B), 8.0–8.1 min (95–70 % B) and 8.1–10 min (70 % B). The flow rate was 1.6 mL/min, and the column temperature was 35 °C. Chromatograms were registered at a wavelength of 220 nm. Quantitative analyses were performed using the calibration curve for the following cannabinoids: CBDA, CBGA, CBD, CBG and THCA (Merck, Germany). An example of cannabinoids separation, standards and a representative sample is reported in Fig. S1.

2.2.3. Terpene analyses

Terpene content was processed following Dei Cas et al. (2021). Each sample (100 mg of freeze-dried inflorescences) was analysed using a Dani Master HS-GC system, with a split-splitless injection and a Dani Master Time-of-flight (TOF) Plus detector in electron ionization mode

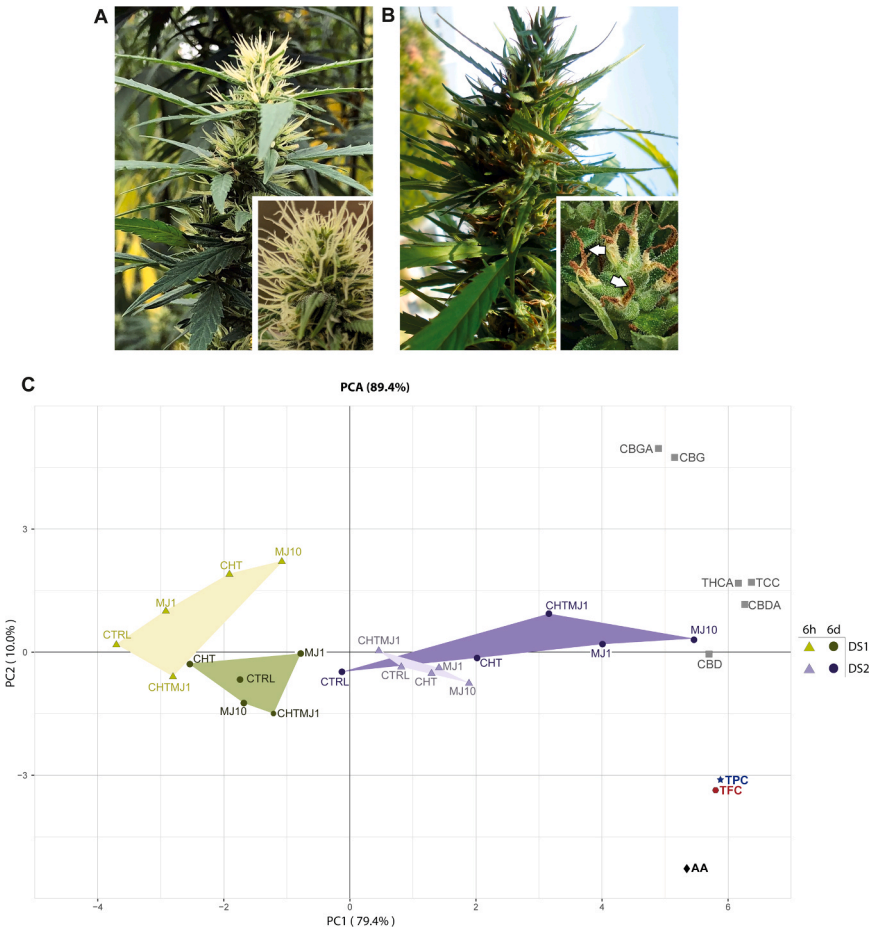

Fig. 1. A-B) Phenotypes of hemp inflorescence at DS1 (**A**) and DS2 (**B**) stages. Arrows indicate mature brown stigmas. **C**) PCA showing the distribution of total phenolic content (TPC), total flavonoid content (TFC), antioxidant activity (AA), total cannabinoid content (TCC) and cannabinoids quantified in *C. sativa* inflorescences from early (DS1, green areas) and mature (DS2, purple areas) developmental stages and harvested at 6 h (HT1, lighter areas) or 6 days (HT2, darker areas) after treatments. CTRL, untreated plants; CHT, chitosan nanoparticles; CHTMJ1, chitosan nanoparticles charged with 1 mM MeJA; MJ1, 1 mM MeJA; MJ10, 10 mM MeJA. CBD, cannabidiol; CBDA, cannabidiolic acid; CBG, cannabigerol; CBGA, cannabigerol acid; THCA, tetrahydrocannabinolic acid.

(70 eV), provided with a DB-5MSUI capillary column. The MS detector operated in full scan mode (*m/z* 40–300) at 5 spectra/s.

2.3. RNA-seq analysis

Total RNA was extracted from 60 frost-stored inflorescences (same samples as for biochemical quantifications) using the RNeasy Plant Mini Kit (Qiagen), followed by DNAse I digestion and RNA quality assessment. Libraries were prepared using the Universal Plus mRNA-Seq kit (Tecan Genomics, USA) and assessed with Qubit 2.0 fluorometer and BioAnalyzer 2100. Sequencing was performed on NovaSeq 6000 in paired-end 150 bp mode. Raw data quality was assessed and cleaned using FastQC v0.11.9 and Trimmomatic v0.39 (Bolger et al., 2014), respectively. High-quality reads were aligned to the CBDRx (cs10, GCF_900626175.2) reference genome using HISAT2 v2.2.1 (Kim et al., 2019). Transcript assembly and expression quantification were performed using StringTie v2.1.5 (Pertea et al., 2015). Transcript-level expression estimes were aggregated into gene-level counts, using the R package 'tximport' v.1.3.2 and subsequently imported into DESeq2 v1.32.0 (Love et al., 2014) for differential expression analysis. Genes with an absolute $\log_2$ fold change ≥ 1 and a false discovery rate ≤ 0.05 were considered differentially expressed (DEGs). Raw counts were normalized using the *DESeq2* and expression levels quantified into transcripts per million (TPM). Genes were considered expressed if their expression level exceeded a threshold of 1 TPM in at least 90 % samples. Finally, the 'enricher' function of the Clusterprofiler v4.0.5 (Wu et al., 2021) package was used to identify gene ontology (GO) terms and Kyoto Encyclopedia of Genes and Genomes (KEGG) pathway annotations enriched for DEGs (corrected p-value $\leq$0.05).

2.4. Gene annotations

GO terms and metabolic pathway annotations were retrieved from the NCBI and KEGG repositories, respectively. To identify and annotate genes involved in targeted secondary metabolites, a combination of literature data, keyword-based searches in the GO and KEGG databases, and protein homology searches (BLASTp v2.12.0 +) against the sequences stored in the NCBI Refseq database were performed. Significant hits were considered with a minimum sequence identity of 70 % and an E-value threshold of $\leq$ 1e-5.

2.5. Weighted Gene Co-expression Network Analysis (WGCNA)

Raw counts from 60 (2 DS x 2 HT x 5 treatments x 3 replicates) or 30 (2 DS x 1 HT x 5 treatments x 3 replicates) samples were variance-stabilised using DESeq2 'varianceStabilizingTransformation' tool. Genes with TPM $<$ 1 in more than 90 % of samples were excluded. The remaining datasets were analysed by the WGCNA R (Langfelder and Horvath, 2008) package using a signed hybrid approach for module detection and network construction, prioritizing positive correlations while allowing weak negative correlations for network balance. Parameters were set as 'Soft Threshold (power) 22', 'minModuleSize 30', and 'mergeCutHeight 0.25'. The resulting networks were named "WGCNA-60" and "WGCNA-30".

2.6. Statistical analyses

All statistical analyses were performed using R software (v4.2.2). Significance thresholds were set at $p \leq 0.05$ unless otherwise stated. The 'aov' function in R was used to perform the analysis of variance (ANOVA) on the biochemical data. Significant ANOVA results were followed by Tukey's HSD test using the 'HSD.test' function from the "agricolae" package (v1.3–7). PCA was performed on mean-centred and standardized data (unit variance scaling) using the 'prcomp' function and visualised as biplots of scores (treatments) and loadings (variables) using the "factoextra" package (v1.0.7). Pearson correlations were calculated using the 'rcorr' function in the Hmisc package (v5.2–3).

2.7. Gene Co-expression Network (GCN) construction and analysis

For GCNs construction, only genes with a module membership score $\geq$ 0.8 in the WGCNA-60 modules were selected to perform pairwise correlation analysis of the expression values from the biological triplicates (60 RNA-seq samples in total). TPM (Transcript Per Million) values were used, log-transformed using $\log_2(x + 1)$ for normalization, and Pearson pairwise correlation analysis was conducted across the selected samples using the "corrplot" and "hclust" packages of R software. Significant correlations (p-value $\leq$ 0.05), with a Pearson's correlation coefficient (r) $\geq |0.8|$ were used to develop the GCNs. Cytoscape software platform v. 3.5.1 (Shannon et al., 2003) was used to visualize the GCN. Topological parameters for gene prioritization were determined using the Cytoscape "NetworkAnalyzer" plugin.

2.8. Reverse Transcriptase Quantitative PCR (RT-qPCR)

First-strand cDNA was synthesised from 1.5 µg of total RNA using the Superscript III first-strand synthesis system (Invitrogen). Primer design was performed using Primer-BLAST software (available at https://www.ncbi.nlm.nih.gov/tools/primer-blast/). qRT-PCR reactions were performed using the Eco Real-Time PCR System (Illumina), following manufacturer's instructions using 50–70 ng of template cDNA, the qPCRBIO SyGreen Blue Mix (Resnova, IT) for template amplification and 400 nM final primers concentration. Two-steps PCR cycling conditions were as follows: 95°C for 5 min, 45 cycles at 95°C for 30 s, 60°C for 30 s, and a final elongation step at 72°C for 5 min. The experiments included three biological and three technical replicates. The *CsEF-1α* gene (LOC115720725) was used for normalization of gene expression.

3. Results and discussion

3.1. Biochemical characterisation of elicited Tiborszallasi hemp inflorescences

Total phenolic content (TPC), total flavonoid content (TFC), antioxidant activity (AA), cannabinoids, and terpenes were determined in *C. sativa* female inflorescences of Tiborszallasi (Fig. 1A-B) from early (DS1) and mature developmental stages (DS2) following treatments with chitosan nanoparticles (CHT), chitosan nanoparticles loaded with 1 mM MeJA (CHTMJ1), 1 mM MeJA (MJ1), 10 mM MeJA (MJ10). Samples were harvested at two time points per each DS: 6 h after treatment (HT1) and 6 days after treatment (HT2). Principal component analysis (PCA) accounted for 89.4 % of the total variance, with PC1 and PC2 explaining 79.4 % and 10.0 % respectively (Fig. 1C).

Specifically, PC1 separated the two DS, and showed a clear distinction between samples harvested at HT1 and HT2 in DS1, whereas a partial overlap between the two HT was observed at DS2. Interestingly, the DS2 samples collected at HT2 showed a clear separation along PC1, which correlated with the increasing MeJA dose. The DS2 HT2 samples treated with 10 mM MeJA were strongly associated with TPC, TFC and cannabinoid contents, and AA levels (Fig. 1C).

3.1.1. Total phenolic content, total flavonoid content, and antioxidant activity

Female inflorescence samples were analysed for TPC, TFC and AA. The TPC showed significant differences for developmental stages (DS1 and DS2), harvest times (HT1 and HT2), treatments (Tr) and the DS × Tr interaction (Table 1). The TPC increased by 36.29 % from DS1 to DS2 (Table S2). Considering the average values of each treatment, 10 mM MeJA elicitation increased TPC by 10.14 % compared to CTRL, and was significantly different from CHT and CHTMJ1 (Table S3). The DS × Tr interaction showed that 1 mM and 10 mM MeJA were more effective in DS2, where TPC increased by 11.56 % and 15.50 %, respectively, over

Table 1
Three-way ANOVA for variance in phenols, flavonoids, antioxidant activity, and cannabinoid acids.

Sources of variation			Phenols	Flavonoids	Antioxidants	Cannabinoids					
DS	HT	Tr	TPC	TFC	AA	CBD	CBDA	CBG	CBGA	THCA	TCC
DS1	6 h	CTRL	20.51 ± 0.36	13.17 ± 2.19 *d*	82.83 ± 3.69 *ef*	0.01 ± 0.00	1.62 ± 0.15 *fg*	0.00 ± 0.00	0.29 ± 0.15	0.13 ± 0.01 *efg*	2.06 ± 0.31 *efg*
		CHT	18.91 ± 0.77	14.93 ± 3.06 *cd*	80.04 ± 3.70 *ef*	0.02 ± 0.00	1.97 ± 0.26 *defg*	0.00 ± 0.00	0.49 ± 0.22	0.17 ± 0.03 *defg*	2.66 ± 0.51 *defg*
		CHTMJ1	21.18 ± 0.27	17.33 ± 3.16 *bcd*	109.82 ± 8.80 *bcdef*	0.01 ± 0.00	1.32 ± 0.47 *defg*	0.00 ± 0.00	0.34 ± 0.09	0.11 ± 0.04 *g*	1.79 ± 0.60 *g*
		MJ1	19.95 ± 0.28	15.53 ± 0.42 *cd*	79.83 ± 8.82 *ef*	0.01 ± 0.00	1.45 ± 0.09 *g*	0.01 ± 0.00	0.35 ± 0.05	0.12 ± 0.00 *fg*	1.94 ± 0.14 *efg*
		MJ10	22.02 ± 0.42	14.83 ± 4.25 *cd*	79.42 ± 21.47 *ef*	0.02 ± 0.01 *defg*	2.25 ± 0.40	0.01 ± 0.00	0.50 ± 0.17	0.21 ± 0.04 *cdefg*	2.99 ± 0.54 *cdefg*
	6 d	CTRL	25.18 ± 0.23	17.93 ± 2.94 *bcd*	106.36 ± 3.50 *bcdef*	0.01 ± 0.00 *fg*	1.59 ± 0.19	0.00 ± 0.00	0.37 ± 0.18	0.13 ± 0.01 *efg*	2.11 ± 0.27 *defg*
		CHT	22.95 ± 1.10	15.37 ± 1.53 *cd*	93.39 ± 11.99 *def*	0.01 ± 0.00	1.44 ± 0.50 *g*	0.00 ± 0.00	0.30 ± 0.19	0.12 ± 0.05 *g*	1.87 ± 0.73 *fg*
		CHTMJ1	25.35 ± 1.02	19.90 ± 2.21 *abcd*	110.41 ± 9.70 *bcdef*	0.02 ± 0.00	1.91 ± 0.17 *g*	0.00 ± 0.00	0.32 ± 0.03	0.16 ± 0.02 *defg*	2.41 ± 0.19 *defg*
		MJ1	25.48 ± 1.63	17.90 ± 3.90 *bcd*	113.10 ± 7.89 *bcde*	0.02 ± 0.01 *efg*	1.79 ± 0.30	0.00 ± 0.00	0.47 ± 0.24	0.15 ± 0.02 *defg*	2.43 ± 0.48 *defg*
		MJ10	25.26 ± 1.57	17.20 ± 0.20 *bcd*	108.13 ± 1.88 *bcdef*	0.02 ± 0.01 *efg*	1.83 ± 0.39	0.00 ± 0.00	0.31 ± 0.11	0.15 ± 0.02 *defg*	2.31 ± 0.52 *defg*
DS2	6 h	CTRL	26.96 ± 3.38	20.27 ± 2.66 *abc*	121.06 ± 21.57 *abcd*	0.02 ± 0.01 *cdefg*	2.69 ± 0.30	0.01 ± 0.01	0.37 ± 0.18	0.21 ± 0.02 *cdefg*	3.30 ± 0.34 *bcdefg*
		CHT	29.71 ± 1.11	20.03 ± 0.12 *abcd*	133.15 ± 8.71 *abc*	0.02 ± 0.00 *bcdef*	2.88 ± 0.66	0.01 ± 0.00	0.50 ± 0.24	0.24 ± 0.06 *bcdefg*	3.65 ± 0.91 *bcdefg*
		CHTMJ1	27.53 ± 1.05	17.27 ± 1.70 *bcd*	110.86 ± 16.01 *bcdef*	0.03 ± 0.00 *bcde*	3.08 ± 0.37	0.01 ± 0.00	0.39 ± 0.02	0.25 ± 0.04 *bcdef*	3.75 ± 0.41 *bcdef*
		MJ1	29.21 ± 0.69	20.63 ± 1.40 *abc*	126.59 ± 11.85 *abcd*	0.02 ± 0.01 *bcde*	3.01 ± 0.73	0.01 ± 0.00	0.49 ± 0.29	0.25 ± 0.08 *bcde*	3.79 ± 1.10 *bcde*
		MJ10	29.41 ± 1.22	20.13 ± 0.75 *abcd*	136.88 ± 3.95 *ab*	0.04 ± 0.01 *cdefg*	2.65 ± 0.22	0.01 ± 0.00	0.37 ± 0.09	0.23 ± 0.02 *bcdefg*	3.30 ± 0.22 *bcdefg*
	6 d	CTRL	30.32 ± 1.62	17.93 ± 2.76 *bcd*	102.45 ± 14.82 *cdef*	0.02 ± 0.00 *cdefg*	2.64 ± 0.69	0.01 ± 0.00	0.30 ± 0.11	0.22 ± 0.05 *cdefg*	3.19 ± 0.81 *cdefg*
		CHT	32.32 ± 0.52	21.10 ± 1.08 *abc*	119.27 ± 3.10 *abcd*	0.02 ± 0.01 *bcd*	3.24 ± 0.81	0.01 ± 0.00	0.45 ± 0.16	0.26 ± 0.07 *bcd*	3.99 ± 1.05 *bcd*
		CHTMJ1	32.16 ± 0.67	20.97 ± 2.10 *abc*	126.99 ± 7.57 *abc*	0.03 ± 0.01 *abc*	3.70 ± 0.62	0.01 ± 0.00	0.76 ± 0.55	0.32 ± 0.05 *abc*	4.82 ± 1.02 *abc*
		MJ1	34.69 ± 1.92	23.70 ± 1.61 *ab*	137.63 ± 5.60 *ab*	0.03 ± 0.00 *ab*	4.13 ± 0.30	0.01 ± 0.00	0.57 ± 0.12	0.36 ± 0.03 *ab*	5.10 ± 0.21 *ab*
		MJ10	36.76 ± 0.60	26.80 ± 0.44 *a*	147.27 ± 9.49 *a*	0.03 ± 0.00	4.71 ± 0.23 *a*	0.02 ± 0.00	0.70 ± 0.15	0.45 ± 0.06 *a*	5.91 ± 0.42 *a*
Signif.		DS	***	***	***	***	***	***	***	*	***
		HT	***	***	***	*n.s.*	**	*n.s.*	*n.s.*	**	**
		Tr	***	*n.s.*	**	**	**	*n.s.*	*n.s.*	***	**
		Ds × HT	*n.s.*	**	**	*n.s.*	***	*	*n.s.*	***	**
		DS × Tr	***	*n.s.*	***	*n.s.*	*n.s.*	*n.s.*	*n.s.*	*n.s.*	*n.s.*
		HT × Tr	*n.s.*	*n.s.*	*n.s.*	*n.s.*	*	*n.s.*	*n.s.*	*	*n.s.*
		DS × HT × Tr	*n.s.*	*	*	*n.s.*	**	*n.s.*	*n.s.*	**	*

Concentrations are expressed as μg GAE/mg DW for TPC, μg CatE/mg DW for TFC, percentage of Inhibition DPPH/mg DW for AA, and percentage of cannabinoids/DW. DS, developmental stage: DS1, inflorescence at early developmental stage; DS2, inflorescence at mature developmental stage; HT, harvest time: 6 h and 6 days post-treatment. Tr, treatment: CHT, chitosan nanoparticles; CHTMJ1, chitosan nanoparticles with 1 mM MeJA; MJ1, 1 mM MeJA; MJ10, 10 mM MeJA. Abbreviations: CBD, cannabidiol; CBDA, cannabidiolic acid; CBG, cannabigerol; CBGA, cannabigerolic acid; THCA, tetrahydrocannabinolic acid; TCC, total cannabinoid content; TPC, total phenol content; TFC, total flavonoid content; AA, antioxidant activity; Tr, treatment; ±, standard deviation (SD); n.s., non-significant; *, **, *** = significant at $P \leq 0.05$, 0.01 and 0.001 respectively. Significance letters are given for the highest level of interaction (DS × HT × Tr).

CTRL (Table S4). Notably, at DS2 HT2, 10 mM MeJA resulted in a 21.24 % higher TPC than control (Table S5).

The ANOVA results of TFC showed significant effects of DS and HT (Table 1). TFC mean values increased by 27.24 % in DS2 over DS1 (Table S2). DS2 × HT2 interaction resulted in a significant enhancement compared to DS1 at both HT1 and HT2 (Table S6). At DS2 HT2, 10 mM MeJA treatment enhanced TFC by 49.47 % with respect to the control (Table S5).

The AA highlighted significant differences for DS, HT, Tr and for most interactions (Table 1). AA rose by 31.02 % from DS1 to DS2, and by 9.85 % from HT1 to HT2 (Table S2). The 10 mM MeJA led to 14.30 % more AA than control (Table S3). The DS × Tr interaction revealed a 27.13 % increase in AA for 10 mM MeJA compared to CTRL in DS2 (Table S4). Noteworthy, AA grew by 43.75 % at DS2 HT2 compared to control (Table S5). The DS × HT × Tr interaction confirmed significant MeJA effects (1 mM and 10 mM) at DS2 HT2 with respect to the CTRL (Table 1).

Overall, DS, HT, and 10 mM MeJA emerged as key factors driving TPC, TFC, and AA increases, except for TFC, where the treatment was significant only at DS2 × HT2.

Developmental stage, genotype and pedoclimatic conditions are known to affect the phytochemical composition of several plant species, including hemp (Trono, 2024). In addition, polyphenol accumulation and increased AA were observed during flower development (Trono, 2024). Our TPC data for mature Tiborszallasi inflorescences (CTRL of DS2, HT2) are in line with those reported by Izzo et al. (2020). Elicitation, a promising strategy to improve the accumulation of secondary metabolites, has been effective in hemp both for *in vitro* cultures and in

plants grown under controlled conditions (Beleggia et al., 2023; Gabotti et al., 2019; Mirzamohammad et al., 2021). Specifically, 10 mM MeJA treatment increased TPC, TFC and AA by 21.24 %, 49.47 % and 43.75 %, respectively (Table S5), further enhancing the upward trend already observed during flower maturation.

Conversely, no significant increase was observed with CHT nanoparticles alone or loaded with 1 mM MeJA. Beleggia et al. (2023) found that chitosan (low, medium, and high molecular weights) significantly increased TPC and AA in hemp inflorescences (Beleggia et al., 2023). The lack of efficacy in our experiments with chitosan nanoparticles was probably due to the 5 mg/L final concentration, which was ten times lower than that used by Beleggia et al. (2023). Furthermore, even when loaded with 1 mM MeJA, nanoparticles had no effect, although 1 mM MeJA alone increased TPC, at least in DS2. Most studies demonstrating the effectiveness of nanoparticles as elicitors have been done on *in vitro* or hydroponically grown plants, suggesting that these conditions may be more suitable for nanoparticle application than foliar spray (Jadoon et al., 2024; Mmereke et al., 2024).

3.1.2. Cannabinoid and terpene contents

The analysis of cannabinoids was performed on the same inflorescence samples. In plants, the main proportion of cannabinoids is represented by the acidic form since decarboxylation occurs upon heating after harvesting (Trono, 2024). As highlighted in Table 1, CBDA, CBGA and THCA were the most abundant compounds, while their decarboxylated form remained below 0.03 %. CBDA and THCA showed significant differences across DS, HT and Tr, whereas CBGA was only affected by DS.

Namely, DS2 led to a 90.12 % and 86.67 % increase in CBDA and THCA mean values, respectively, compared to DS1 (Table S2). 10 mM MeJA was the most effective treatment, raising CBDA and THCA by 33.64 % and 52.94 %, respectively (Table S3). Interestingly, in mature inflorescences harvested after 6 days post-treatment (DS2, HT2), CBDA increased by 4.71 %, representing a rise of 78.41 % compared to untreated samples, whereas THCA doubled to 0.45 % but never exceeded the legal 0.6 % limit (Table 1, Table S5). Variance analysis for TCC showed the same significance as the main cannabinoids (Table 1).

Recently, Yang et al. (2020) described cannabinoid accumulation in industrial hemp during flower development, reporting an increase at progressive stages (Yang et al., 2020). Our field-grown Tiborszallasi female inflorescences followed the above-described cannabinoid accumulation trend. While studies on elicitation with signal molecules mainly focus on chemotypes I and II, less is reported about chemotype III (Trono, 2024).

Overall, our results suggest that MeJA effectively elicits cannabinoids accumulation depending on concentration. Our data highlighted a significant CBDA and THCA increase with 10 mM MeJA treatment, whereas chitosan nanoparticles, both charged and uncharged (Table 1), had no significant effect, consistent with previous observations (Beleggia et al., 2023).

Considering that the greatest impact of the elicitor was noticeable in inflorescences harvested at 6 days post-treatment, total terpene content (TTC) analysis was performed only at HT2 on DS1 and DS2 samples. A total of 17 terpenes were identified, and six compounds (four monoterpenes and two sesquiterpenes) present in all samples were selected for ANOVA (Table 2). TTC significantly increased with flower development (DS2) and after 1 mM and 10 mM MeJA treatments (Table 2). Specifically, TTC increased by 37.6 % in DS2 over DS1 (Table S7). MeJA elicitation led to an average TTC increase of 51.8 % (1 mM) and 69.7 % (10 mM) over control. In DS2, 1 mM and 10 mM MeJA increased TTC levels by 82.1 % and 94.7 %, respectively (Table S7). The DS × Tr interaction significantly affected β-ocimene, with the 10 mM treatment differing from all samples except 1 mM MeJA (Table 2). Indeed, β-Ocimene is one of the most common volatiles emitted after wounding, biotic stress and jasmonic (Fäldt et al., 2003). Table 2 shows that DS had a stronger effect on monoterpenes than on sesquiterpenes. Our findings align with previous studies (Aizpurua-Olaizola et al., 2016) reporting that monoterpenes levels increased, whereas sesquiterpenes levels declined during flower development. This decline could be explained by the interaction between the biosynthetic pathways of terpenes and cannabinoids. Both pathways have in common the formation of isopentenyl diphosphate (IPP) and dimethylallyl diphosphate (DMAPP). The condensation of one DMAPP and one IPP molecule forms geranyl diphosphate (GPP), a monoterpenes precursor, whereas the condensation of one DMAPP and two IPP leads to farnesyl diphosphate (FPP), the sesquiterpenes precursor. Our results showed that cannabinoids and monoterpenes synthesis is favored over sesquiterpenes production, suggesting that different stages of plant development could result in different terpenes content. Regarding elicitation, monoterpenes were affected by MeJA treatment but not by the other elicitors, which is consistent with the results for cannabinoids. Moreover, a clear relationship between cannabinoids and terpenes content emerged (Booth et al., 2020).

3.2. Transcriptomic responses to eliciting treatments

3.2.1. Transcriptome sequencing and differential expression analysis

The transcriptome response to different treatments was assessed using the same inflorescence samples as in biochemical profiling. A total of 60 paired-end libraries were generated, with an average sequencing depth of ca. 72.5 million reads *per* sample (range: 57–126 million), and over 98.4 % of reads passed quality controls. Successful alignment to the

Table 2
Monoterpene and sesquiterpene contents at HT2 and two-way ANOVA significances.

Sources of variation		Terpenes (ppm)						
DS	**Tr**	**aPNN**	**bPNN**	**LMN**	**bOC**	**aHML**	**bCPN**	**TTC**
DS1	CTRL	563.2 ± 38.0	196.3 ± 41.4	31.5 ± 20.5	267.1 ± 104.9 *bc*	342.0 ± 35.4	890.1 ± 108.0	2290.3 ± 56.1
	CHT	622.4 ± 242.2	229.6 ± 63.4	16.6 ± 4.3	65.8 ± 3.7 *bc*	333.3 ± 160.6	868.5 ± 301.6	2136.2 ± 550.1
	CHTMJ1	808.7 ± 219.9	225.3 ± 65.2	16.1 ± 0.4	50.2 ± 7.4 *c*	611.6 ± 182.9	1235.0 ± 222.3	2946.9 ± 548.6
	MJ1	860.6 ± 265.2	251.0 ± 107.3	17.5 ± 6.4	145.2 ± 11.0 *bc*	409.7 ± 159.7	1057.2 ± 473.8	2741.3 ± 434.0
	MJ10	969.1 ± 266.9	303.0 ± 94.3	38.6 ± 17.3	126.4 ± 93.4 *c*	537.2 ± 46.7	1304.4 ± 150.7	3278.6 ± 392.9
DS2	CTRL	804.7 ± 251.3	286.6 ± 142.5	84.7 ± 1.6	44.9 ± 21.7 *c*	445.2 ± 362.9	764.3 ± 703.9	2430.3 ± 835.9
	CHT	1779.7 ± 423.8	559.2 ± 68.0	27.0 ± 13.8	191.4 ± 98.5 *bc*	219.8 ± 18.0	602.3 ± 43.3	3379.4 ± 527.8
	CHTMJ1	1870.7 ± 664.8	584.2 ± 230.1	25.8 ± 10.6	24.5 ± 8.8 *c*	258.3 ± 29.3	699.7 ± 105.1	3463.3 ± 1022.3
	MJ1	1740.8 ± 722.7	697.6 ± 359.8	33.6 ± 14.6	742.1 ± 439.4 *ab*	331.8 ± 40.8	880.4 ± 227.4	4426.3 ± 664.0
	MJ10	1758.4 ± 425.4	594.5 ± 186.6	58.1 ± 50.6	1023.2 ± 475.6 *a*	376.2 ± 145.2	921.1 ± 366.6	4731.4 ± 304.0
Signif.	DS	***	***	**	**	*	*	***
	Tr	*	*n.s.*	**	**	*n.s.*	*n.s.*	***
	DS × Tr	*n.s.*	*n.s.*	*n.s.*	**	*n.s.*	*n.s.*	*n.s.*

DS, developmental stage; Tr, treatment. Abbreviations: aPNN, α-Pinene; bPNN, β-Pinene; LMN, D-Limonene; bOC, β-Ocimene; aHML, α-Humulene; bCPN, β-Caryophyllene; TTC, total terpene content; ±, standard deviation (SD); n.s., non-significant; *, **, *** = significant at P ≤ 0.05, 0.01 and 0.001 respectively. Significance letters are given for the highest level of interaction (DS × Tr).

reference genome ranged from 76.0 % to 92.1 %, with 64.6–81.0 % uniquely mapped (Fig. S2A). PCA of RNA-seq data (Fig. S2B) revealed DS1 samples clustering separately from DS2 along PC1 (40 % variance), whereas HT1 separated from HT2 along PC2 (11 % variance). MeJA perception in inflorescences was confirmed by the transcriptional activation of JA pathway and signaling genes (Fig. S3A; Table S8), consistent with previous work on MeJA-treated hemp (Fayaz et al., 2023; Welling et al., 2023). At DS1 HT1, three, fifteen and two genes were induced by MJ1, MJ10 and CHTMJ1, respectively. At DS2 HT1, four, ten and two marker genes showed transcriptional variation in response to MJ1, MJ10 and CHTMJ1, respectively (Fig. 2A, Fig. S3B). Notably, no MeJA marker genes were activated at HT2 or in response to CHT treatments at any developmental stage. Within DS1, HT1 inflorescences showed about twice as many DEGs as HT2 (678 *vs* 383), independently of treatment (Fig. 2B, left panel). At DS2, DEG counts were similar across harvest times (656 *vs* 648; Fig. 2B, right panel). MJ1 and MJ10 affected more genes than CHT and CHTMJ1 at both DS (Fig. 2B, Table S8). Additionally, at HT1, MeJA-treated inflorescences had more upregulated than downregulated genes, whereas the opposite trend was observed at HT2. At both DS, total DEG count increased with the MeJA dose. In summary, hemp inflorescences exhibited a stronger transcriptional response to MeJA at early growth stages, in a dose-dependent manner, with rapid stimulus perception, consistent with other studies (Matthes et al., 2008; Wang et al., 2023; Welling et al., 2023). MeJA-induced gene activation ranged from 0.5 h to several hours in plant species (Shi et al., 2015; Wei, 2010), with long-lasting effects mediated by downstream signalling cascade (Bahieldin et al., 2018).

3.2.2. Functional enrichment analyses

The biological functions of DEGs were investigated through GO term and KEGG pathway enrichment analyses. In GO analysis (Fig. 2C, Fig. S4), more enriched terms were identified at DS1 compared to DS2, where enrichments were restricted to MJ1, MJ10, and CHT treatments. Biological process terms related to jasmonic acid metabolism ('jasmonic acid metabolic process'; 'regulation of jasmonic acid mediated signalling pathway'), salicylic acid metabolism ('salicylic acid metabolic process') and stress response ('regulation of defence response'; 'response to wounding') were enriched in HT1 samples supplied with MJ1, MJ10 or CHTMJ1 at DS1, and with MJ10 at DS2. These results agree with MeJA role in JA biosynthesis regulation and secondary metabolism activation via a salicylic acid-dependent network (Hickman et al., 2017). In metabolic pathway analysis (Fig. 2D), at DS1, enrichment was mainly observed at HT1 (except for CHTMJ1), whereas at DS2, the most enriched pathways were observed at HT2. At DS1, MJ1 significantly affected carbohydrate metabolism ('starch and sucrose'; 'pentose and glucuronate interconversions'; 'galactose metabolism'), while MJ10 altered polyunsaturated fatty acids (PUFAs) pathways ('linoleic acid metabolism'; 'α-linolenic acid metabolism'). At DS2, MJ1 influenced phenolic compound metabolism ('phenylpropanoid biosynthesis'; 'stilbenoid, diarylheptanoid and gingerol biosynthesis'), while MJ10 modified the 'flavonoid biosynthesis' pathway. Although starch and sucrose metabolism were previously reported to be altered by MeJA in sorghum with impact on floret opening (Liu et al., 2021), transcriptional changes in PUFAs and phenolic metabolism are more commonly observed after MeJA applications (Cao et al., 2017; Gabotti et al., 2019; Pauwels et al., 2008; Shi et al., 2015; Yao et al., 2021). Linoleic and α-linolenic acids are key structural components of plant cell membranes, play a pivotal role in stress responses, and are primary JA precursors (Graña et al., 2020). In this work, 48 genes were annotated in the 'alpha-linolenic acid metabolism' pathway of *C. sativa*, and 8 were significantly up-regulated at DS1 in MJ10-treated samples at HT1 (Fig. S3B). These included three *lipoxygenases* (*LOX*: *LOC115719614*, *LOC115719616*, *LOC115720530*), two *allene oxide synthase* (*AOS*: *LOC115703182*, *LOC115723125*) genes, the *acyl-coenzyme A oxidase 1* (*ACX1*: *LOC115715988*), *12-oxophytodienoate reductase* (*OPR*: *LOC115722904*), and jasmonate O-methyltransferase (*JMT*: *LOC115701091*) genes. These *LOX*, *AOS* and *OPR* gene families have been implicated in stress responses, growth, and development in *C. sativa* (Borrego et al., 2023; Fayaz et al., 2023; Welling et al., 2023), with some genes specifically MeJA-induced, as observed in this work (Fig. S3B). *JMT* encodes an enzyme catalyzing JA methylation to MeJA (Seo et al., 2001), and in our dataset, its expression at DS1, 6 h after the MJ10 treatment, was the highest among all pathway genes (Fig. S3B, Table S8) consistent with previous observations in hemp (Welling et al., 2023). MeJA-induced JA biosynthetic gene expression is a key component of the positive feedback loop regulating jasmonate levels (Zhu et al., 2024). This is further supported by studies on JMT-overexpressing plants, which exhibit increased endogenous MeJA, activation of phenylpropanoid and tyrosine-derived pathways, and phenolic and flavonoid accumulation (Seo et al., 2001; Wang et al., 2018). These results showed that at DS1, MeJA primarily modulates pathways related to primary metabolism (carbohydrates and polyunsaturated fatty acids) and its own synthesis, whereas at DS2, MeJA treatments shift the transcriptional focus toward secondary metabolite biosynthesis.

3.2.3. Target gene pathways

A total of 384 genes linked to 10 biosynthetic pathways involved in secondary metabolites (quantified in this study) were identified in the reference genome (Table S8). These pathways (Table 3) included hexanoic acid and cannabinoid biosynthesis (HEX, CAN), aromatic and phenolic compounds (SHK, PHP, FLA, ISO), and terpenes (TER, MTP, DTP, STP). Approximately 69 % of these genes had a transcript abundance of at least 1 TPM (Transcripts per Million) in 90 % or more of the samples and were included in the differential expression analysis.

Here, we report on gene transcription patterns within the mentioned pathways in response to varying factors (Fig. 3A, Table S8). Overall, the MeJA treatments (MJ1, MJ10) altered the expression of more genes than those affected by the chitosan-containing treatments (CHT and CHTMJ1). With respect to DS1 at HT1, CHT did not alter the expression of any target gene, both MJ1 and CHTMJ1 affected a modest number of genes (2 DEGs each), whereas MJ10 affected on 11 DEGs. In DS1 at HT2, DEGs were observed with MJ1 (2), CHT (1) and CHTMJ1 (1) and MJ10 (6), this latter remaining the most effective in terms of whole number of affected genes. Looking at DS2 HT1, both MJ1 and MJ10 had the highest impact by producing 7 and 15 DEGs, with a swapped trend at HT2 (respectively 23 and 9 DEGs) but maintaining the highest effect among all treatments.

Looking at the phenylpropanoid pathway, gene expression changes occurred for all MeJA-based treatments (MJ1, MJ10 and CHTMJ1), except for the combination DS1/MJ1 at HT2, with MJ1 and MJ10 producing the highest number of DEGs respectively at DS2 HT2 (13 DEGs) and DS2 HT1 (10 DEGs). A total of 191 genes were assigned to the phenylpropanoid pathway, accounting for 13 distinct enzymatic activities (Table 3; Table S8) and its DEGs number induced by MJ1 and MJ10 varied with the developmental stage and time after treatment. All DEGs associated with hydroxycinnamic acid and monolignol biosynthesis (Fig. 3B) and belonged to the *CYP98A (C3'H)*, *cinnamyl-alcohol dehydrogenase* (*CAD*), *caffeic acid 3-O-methyltransferas* (*COMT*), *hydroxycinnamoyl transferase* (*HCT*), and *peroxidase* (*PRX*) gene families. Most of them exhibited up-regulated expressions (Fig. 3C), suggesting a global transcriptional boost of the phenylpropanoid biosynthesis pathway. MeJA-induced changes in gene expression within the phenylpropanoid pathway have been extensively documented in different plant species, growth conditions and target organs or tissues. These alterations are often linked to the accumulation of secondary metabolites, including phenolics, flavonoids, hydroxycinnamic acids, monolignols, and terpenes.

In *Arabidopsis* cell cultures, MeJA elicitation significantly upregulated genes involved in phenylpropanoid and monolignol biosynthesis (Pauwels et al., 2008). Similarly, in *Carthamus tinctorius* inflorescences, MeJA directly activated an *HCT* promoter and stimulated flavonoid accumulation (Chen et al., 2020) while safflower cell cultures showed

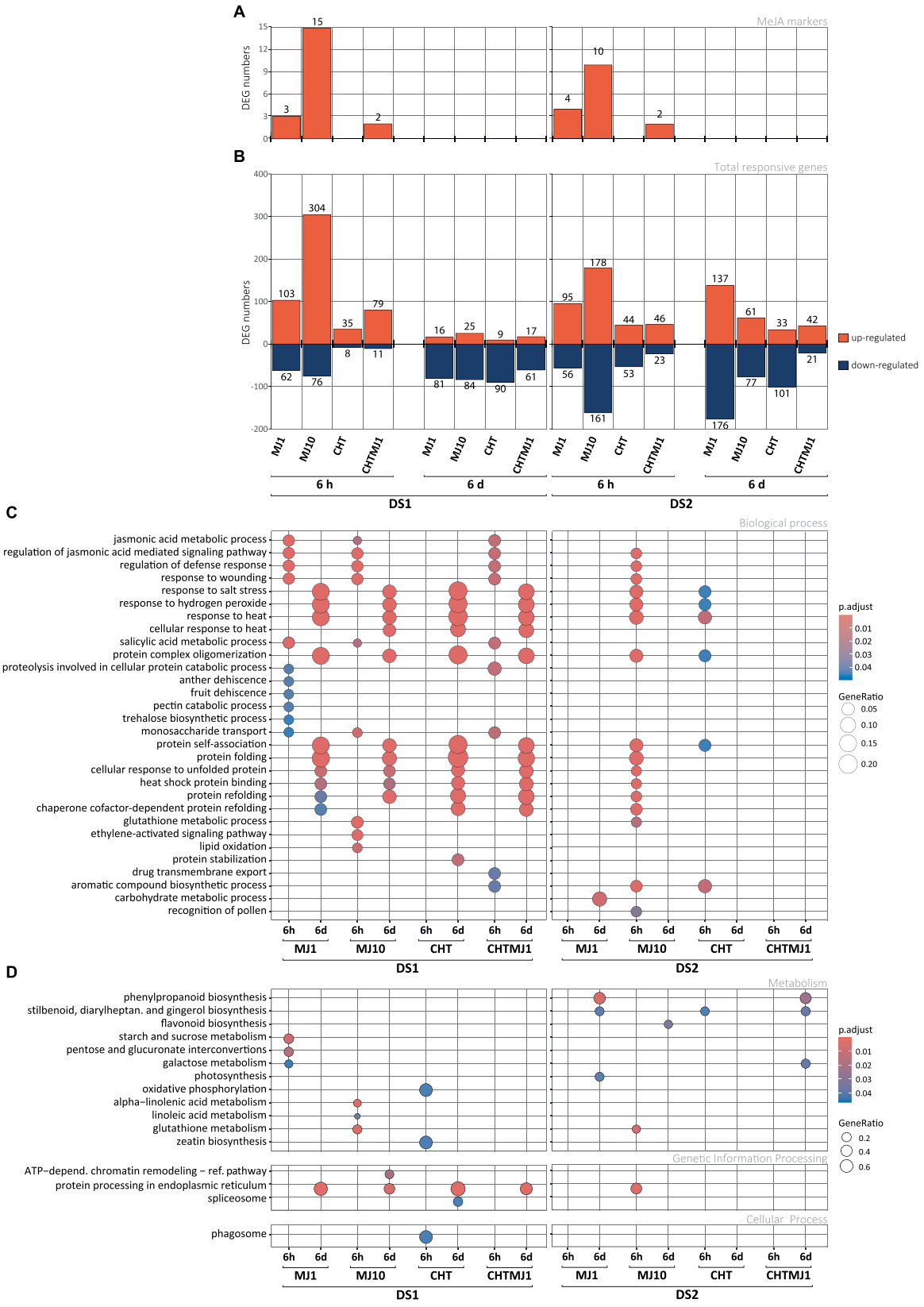

Fig. 2. Total number of DEGs in hemp inflorescences in response to treatments. **A-B**) Bar plots showing the number of DEGs (y-axis) in treated vs untreated plants at both 6 h (6 h, HT1) and 6 days (6 d, HT2) post-treatments (x-axis). **A**) Number of MeJA-marker genes in inflorescences at early (DS1; left panel) and mature (DS2; right panel) developmental stages. **B**) Total number of up- and down-regulated genes (orange and blue bars, respectively) in each treatment as compared to control in DS1 (left panel) and DS (right panel). The number of DEGs is given at the top of each bar. **C-D**) GO and KEGG enrichment analyses. **C**) Dot plots showing significantly enriched GO terms (y-axis) for each combination (x-axis) of developmental stage (DS), treatment (**Tr**) and harvest time (HT). **D**) Dot plots showing the metabolic pathways (y-axis) enriched in DEGs for each combination of DS, **tr** and HT (x-axis), grouped according to KEGG macro-categories.

Table 3
Pathways and number of annotated genes.

Metabolic pathways	Abbreviations	n. genes
Hexanoic acid	HEX	5
Cannabinoids	CAN	16
Shikimate	SHK	37
Phenylpropanoids	PHP	191
Flavonoids	FLA	76
Isoflavonoids	ISO	9
Terpenoid backbone	TER	26
Monoterpenes	MTP	18
Diterpenes	DTP	20
Sesquiterpenes	STP	31
	Total[1]	**429**

1, Note: PHP and FLA share 45 genes.

MeJA-induced *HCT* up-regulation and accumulation of hydroxycinnamic acids (Liu et al., 2024), highlighting commonalities among upstream steps in phenylpropanoid and flavonoid pathways. In *C. sativa*, MeJA applications altered the expression of phenylpropanoid-related genes, resulting in increased production of phenolic compounds and enhanced antioxidant activity in cell cultures (Gabotti et al., 2019), and promoted the monolignol biosynthesis pathway at both transcriptional and metabolic levels in hemp hypocotyls (Behr et al., 2019). Regarding cannabinoids, *OLS* gene (*LOC115700696*) was induced by MJ10 at DS2 HT2 (Fig. 3A, Table S8), consistent with the ca. 2-fold increased level in THCA and CBDA (Table S5). Interestingly, MeJA-induced cannabinoid accumulation in hemp was reported to occur without major transcriptional changes in cannabinoid biosynthesis genes, such as *OAC, PT4, CBDAS* and *THCAS* (Garrido et al., 2022). For terpenes, although the number of DEGs was modest, *LOC115716064*, encoding a limonene synthase (CsTPS1) with specific functions in hemp glandular trichomes (Conneely et al., 2024), was strongly induced by MJ1 and MJ10 at DS1 HT2. Relatedly, MeJA stimulation of triterpenoid biosynthesis has been observed in hemp hairy root cultures (Kobtrakul et al., 2023). Moreover, jasmonate-responsive transcription factors (e.g. MYC2) can regulate downstream pathways critical for monoterpenes and sesquiterpenes synthesis (Zulak et al., 2009). Taken together, these results confirm the role of MeJA in mediating stress conditions through the activation of early response genes and the triggering of a regulatory transcriptional cascade leading to late defence-related responses, in which phenylpropanoid metabolism plays a central role.

3.3. WGCNA and GCN analyses identified two main anticorrelated transcriptional modules associated to secondary metabolites production

To explore the regulatory transcriptional networks underlying the accumulation of secondary metabolites in response to MeJA elicitation, we applied a weighted gene co-expression network analysis (WGCNA). WGCNA is a systems biology method for describing the correlation patterns among genes across transcriptomic samples, finding clusters (modules) of highly correlated genes that can be related to one another and to external sample traits such as metabolite content (Langfelder and Horvath, 2008)

To this aim, gene expression values from 60 RNA-seq samples were filtered to exclude genes with low abundance expression. The resulting 17223 genes were analysed in the WGCNA using a signed hybrid approach for network construction and module detection, an intermediate approach that aims to balance the advantages of both signed and unsigned networks (Langfelder and Horvath, 2008). The identified co-expression modules were then related to TPC, TFC, AA and individual (CBDA, CBGA, CBG, CBD, THCA) or total cannabinoids content (TCC). The resulting network (Fig. 4A), named WGCNA-60, consisted of 16 modules of highly correlated genes (Table S9). Among them, two modules (Midnightblue and Orange) resulted highly positively correlated, and one (Red) negatively correlated with several secondary metabolites (Fig. 4B). However, the Orange module contained only genes with low (<0.5) module membership (MM) and was not further considered. Differently, the Midnightblue module (2141 genes, including 87 genes related to target metabolites), and the Red module (754 genes, including 8 genes related to the target metabolites) had high MM and were further investigated. TPC and CBDA showed the strongest positive correlation with the Midnightblue ($r = 0.74$ and $r = 0.63$, respectively), and the strongest negative correlation ($r = -0.7$, and $r = -0.68$, respectively) with the Red module (Table S9). Although correlation indexes were lower (ranging from 0.5 to 0.61), the Midnightblue module also showed significant correlation with the content of CBD, THCA, AA, TFC and TCC. CBGA and CBG showed weaker correlations, likely due to their low accumulation as intermediate in the cannabinoid biosynthetic pathway.

We then focused on metabolic genes and transcription factors (TFs) with high MM (hub genes) and high degree of correlation with each secondary metabolite class. High module membership indicates those genes with an expression pattern that is highly representative of the module, and identify them as candidate hubs in a system, with biological and statistical significance. Among genes encoding metabolic enzymes, thirteen genes in the phenylpropanoid, terpene, hexanoic acid and fatty acid biosynthesis pathway displayed MM $\geq$ 0.9 (Table 4) and can be considered hubs in the secondary metabolite accumulations. In particular, in this list are three genes encoding members of the acyl-activating enzyme (AAE) superfamily, which activate carboxylic acids through an adenylate intermediate (Schmelz and Naismith, 2009), and can use phenylpropanoids, fatty acids, and jasmonate precursors as substrates. *CsAAE1* is crucial for activating hexanoic acid to hexanoyl-CoA, the starter molecule for cannabinoid biosynthesis (Stout et al., 2012), whereas the role of *CsAAE5* has not been characterized in the cannabinoid biosynthetic pathway. *CsAAE5* may participate in fatty acid activation, which can contribute to lipid-derived cannabinoid precursors. The presence of another gene potentially contributing to fatty acid metabolism, *Fatty Acid Desaturase 8 (CsFAD8),* which may affect precursor pools like hexanoic acid used in CBGA biosynthesis, point to a prominent role of the fatty acid pathway as a main target for the developmental stage-dependent MeJA elicitation of the cannabinoid biosynthesis. The third member of the AAE superfamily is a gene encoding a 4-Coumarate:CoA ligase *(4CL)*, involved in phenylpropanoid metabolism and the long chain acyl-CoA synthetases. Other two genes, Cs*CSE*, and Cs*ALDH2C4* are involved in the phenylpropanoid pathway, leading to the synthesis of flavonoids and lignin precursors. Among the other identified metabolism hubs, *CsCAD* encoding a berberine bridge enzyme-like that is part of the same family as THCAS, CBDAS, CBCAS, responsible for oxidative cyclization of CBGA to cannabinoids, and a mevalonate kinase gene (*CsMK*), part of the mevalonate pathway, which produces geranyl pyrophosphate (GPP), a precursor to CBGA, the central cannabinoid intermediate.

In Midnightblue module, 41 TFs displayed MM $\geq$ 0.9 (Table 5), with TALE, WRKY, NAC, MYB, ERF and MYB-related families being the most represented. Notably, a TALE gene homologous to the *Arabidopsis BLH1* and an *EIL* gene homolog displayed the highest module membership scores (MM = 0.98). The list of the TFs identified as major hubs for the secondary metabolite production in the WGCNA includes five members of the TALE (Three-Amino acid Loop Extension) TFs. TALEs are encoded by two small subfamilies in the *Arabidopsis thaliana* genome where the sequences of eight KNOX and 13 BELL/BLH genes have been identified (Mukherjee et al., 2009). This transcription factor family has not yet been characterized in hemp, and no TALE transcription factors have previously been described in the context of cannabinoid biosynthesis in *C. sativa*. The identification of five TALE members (two KNOX and three BELL/BLH) suggests a novel and potentially important role for TALEs in hemp inflorescence maturation and active secondary metabolite accumulation. TALE transcription factors play a recognized role in maintaining the fine balance between undifferentiated meristematic function and cell differentiation (Di Giacomo et al., 2013, 2017). Two family

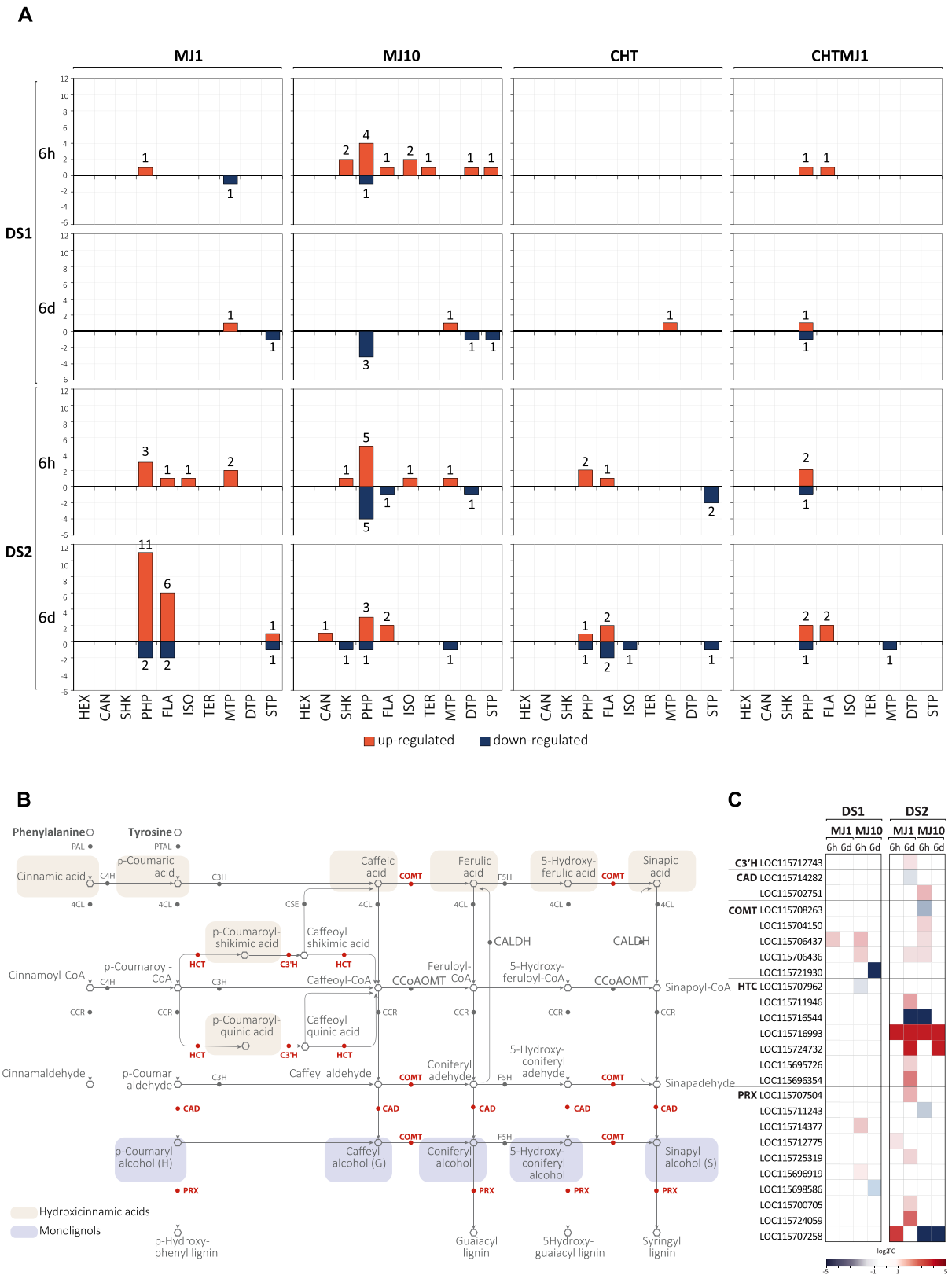

Fig. 3. DEGs in target pathways. **A)** Bar plots showing the number of DEGs (y-axis) across each pathway of interest (x-axis) at 6 h (HT1) and 6 d (HT2) after treatments at the two developmental stages, DS1 and DS2. For each condition, the number of up-regulated (orange bars) and down-regulated (dark blue bars) genes is displayed. Values above the bars indicate the total count of DEGs in each pathway. Pathway abbreviations: CAN, Cannabinoids; DTP, Diterpenes; FLA, Flavonoids; HEX, Hexanoic acid; ISO, Isoflavonoids; MTP, Monoterpenes; PHP, Phenylpropanoids; SHK, Shikimate; STP, Sesquiterpenes; TER, Terpenoid backbone. **B)** Scheme of the biosynthetic circuits of hydroxycinnamic acids (light beige boxes) and monolignols (light lavender boxes). DEGs, regardless of DS, HT and treatments are typed in red. **C**) Heatmap of DEGs within the phenylpropanoid pathway, corresponding to the genes shown in red in panel B.

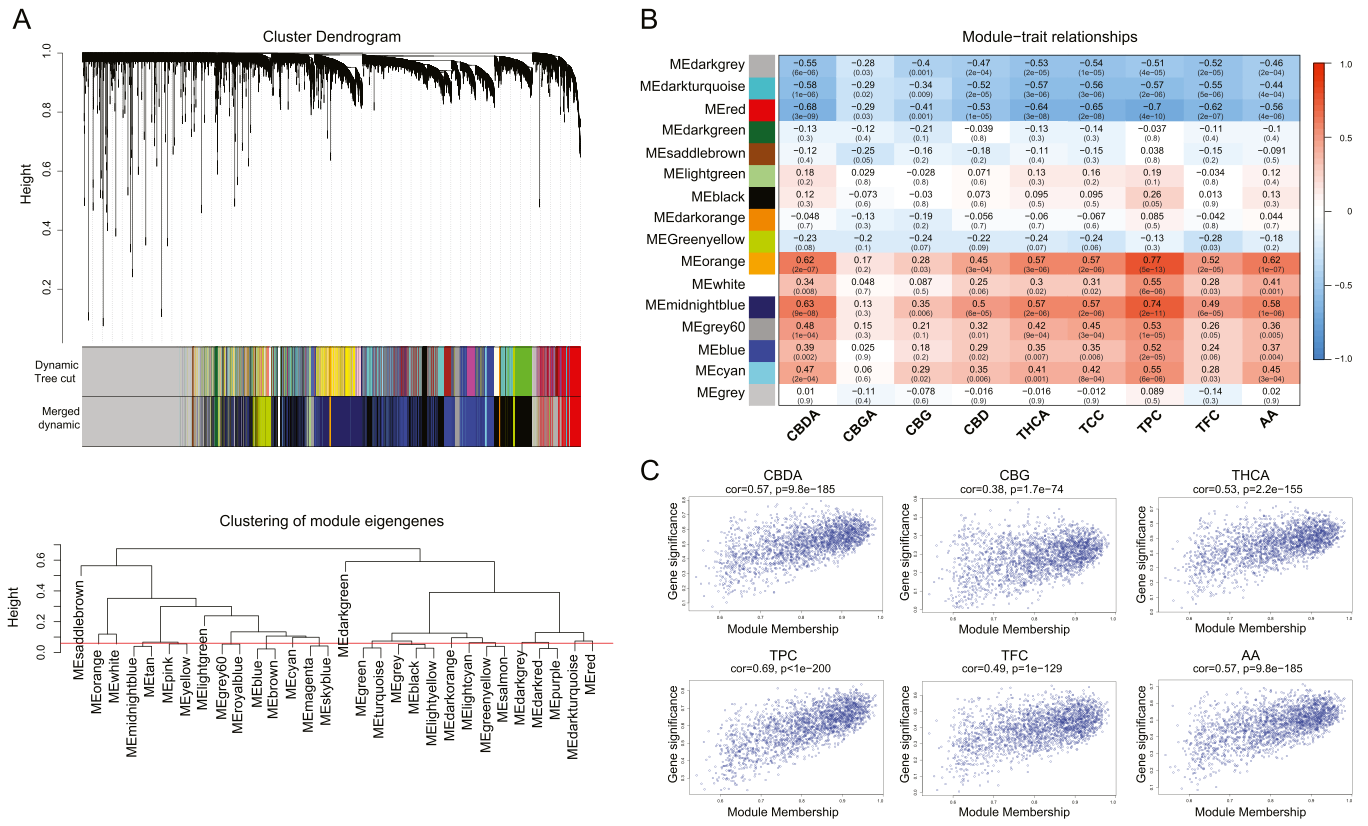

Fig. 4. Gene modules and their correlation to secondary metabolites as identified by WGCNA. **A)** Gene cluster dendrogram obtained by average linkage hierarchical clustering. The colour rows underneath the dendrogram show the initial module assignment determined by the Dynamic Tree Cut (upper row), and the module assignment after merging modules (lower row) whose dissimilarity was below the cutoff indicated in red in the clustering of module eigengenes under the dendrogram. The grey module represents unassigned genes. **B)** The Module-trait relationships represent the correlation between module eigengenes (MEs) and metabolite content in WGCNA: total phenolic content (TPC), individual (CBDA, CBD, CBGA, CBG, THCA) and total cannabinoids content (TCC), antioxidant activity (AA), and total flavonoid content (TFC). Each square contains Pearson's correlation coefficient between the MEs and trait (metabolite) and their associated p-values (in brackets underneath). The red and blue colours show a strong positive and negative correlation, respectively. **C)** The six scatterplots represent the MM in the MEmidnightblue module (x-axis) versus the Gene Significance (GS) (y-axis) for a specific metabolite (CBDA, CBG, THCA, TPC, AA, TFC). Correlations and p-values were calculated: all correlations were significant and varied from 0.38 (CBG) to 0.69 (TPC), indicating a strong association between these metabolites and the genes in the Midnightblue module.

Table 4
Genes belonging to biochemical metabolic pathways with the highest module membership (MM) in the Midnightblue of the WGCNA-60.

Genes	MM	Pathway[1]	Description	Symbol
LOC115699132	0.98	PHP	4-coumarate–CoA ligase-like 7	*4CL*
LOC115711963	0.96	PHP	caffeoylshikimate esterase	*CSE*
LOC115697681	0.96	Fatty acid	fatty acid desaturase 8	*FAD8*
LOC115716315	0.95	HEX	acyl activating enzyme 5	*AAE5*
LOC115697888	0.93	SHK	aspartate aminotransferase, cytoplasmic	*AAT*
LOC115702757	0.92	ISO	isoflavone 3′-hydroxylase	*I2′H*
LOC115698090	0.92	PHP	berberine bridge enzyme-like 13	*CAD*
LOC115714155	0.92	STP	beta-amyrin synthase	*LUP2*
LOC115719471	0.91	TER	mevalonate kinase	*MK*
LOC115707294	0.91	PHP	aldehyde dehydrogenase family 2 member C4	*CALDH*
LOC115705312	0.91	PHP	caffeoylshikimate esterase	*CSE*
LOC115703163	0.91	TER	hydroxy-diphosphate reductase	*HDR*
LOC115713865	0.91	HEX	acyl activating enzyme 1	*AAE1*

1, Pathway abbreviations: HEX, Hexanoic acid; ISO, Isoflavonoids; MTP, Monoterpenes; PHP, Phenylpropanoids; SHK, Shikimate; STP, Sesquiterpenes; TER, Terpenoid backbone.

members of class 2 KNOX in *Arabidopsis*, which homologs are in the list, were shown to synergistically regulate monolignol biosynthesis, and involved in secondary cell wall biosynthesis (Qin et al., 2020). Their role in hemp inflorescences may relate to trichome specialized cell differentiation and lignin metabolism. As for *CsEIN3*, identified together with *CsBLH1* as highly associated to the Midnightblue transcriptional module, no homologs of *EIN3* (*ETHYLENE-INSENSITIVE 3*) have been described in the context of cannabinoid biosynthesis or the regulation of related pathways like trichome development in *Cannabis sativa*. Interestingly, AtEIN3 has been shown to interact with MYC proteins (members of the bHLH transcription factor family) to modulate jasmonate-induced genes, potentially linking this interaction to MeJA-induced responses (Liu et al., 2022). Consistently, a gene encoding a jasmonate ZIM-domain (JAZ) protein correlates with cannabinoid production, further connecting the jasmonate response to the promotion of secondary metabolism. A recent study demonstrated that exogenous application of MeJA positively affects trichome density and the transcript levels of JAZ genes in hemp (Huang et al., 2024). This effect occurs through the upregulation of a MYC transcription factor, *CsMYC4*, which was identified as a key regulator of glandular trichome formation in *C. sativa* via MeJA signalling. We found several bHLH genes in the two anticorrelated modules linked to secondary metabolite production, which may be involved in this regulatory JAZ-MYC-EIN3 regulatory module. JAZ can repress MYC TFs function in the absence of JA, whereas the presence of JA relieves this repression, activating MYC and

Table 5
Genes encoding TFs with the highest module membership (MM) in the Midnightblue of the WGCNA-60.

Genes	MM	TF class	Best Arab. hit	Description
LOC115699161	0.98	TALE	AT2G35940	BEL1-like homeodomain 1 (BLH1)
LOC115706079	0.98	EIL	AT3G20770	Ethylene insensitive 3 family protein
LOC115701065	0.97	WRKY	AT3G58710	AT3G58710
LOC115701358	0.96	NAC	AT1G69490	NAC-like, activated by AP3/PI
LOC115698801	0.96	TALE	AT5G25220	Homeobox protein knotted−1-like 3 (KNAT3)
LOC115699582	0.96	WRKY	AT2G03340	AT2G03340
LOC115701153	0.95	WRKY	AT4G22070	AT4G22070
LOC115715113	0.95	ERF	AT5G13330	related to AP2 6 l
LOC115703078	0.95	C2H2	AT1G27730	AT1G27730
LOC115718987	0.95	WRKY	AT2G38470	WRKY DNA-binding protein 33
LOC115706270	0.95	NAC	AT3G15510	NAC domain containing protein 2
LOC115699157	0.94	bZIP	AT5G06950	Transcription factor of the B-ZIP family
LOC115709772	0.94	NAC	AT5G61430	NAC domain containing protein 100
LOC115714915	0.94	TCP	AT3G27010	TEOSINTE BRANCHED 1, cycloidea,
LOC115716369	0.94	MYB_related	AT5G47390	myb-like transcription factor family protein
LOC115716984	0.93	TALE	AT1G62990	KNOTTED-like homeobox of A. thaliana 7 (KNAT7)
LOC115716934	0.93	TALE	AT5G41410	POX (plant homeobox) family protein (BELL1)
LOC115722074	0.93	CO-like	AT2G47890	AT2G47890
LOC115707725	0.93	WRKY	AT1G62300	WRKY family transcription factor
LOC115712195	0.93	ERF	AT1G46768	AT1G46768
LOC115709433	0.93	WRKY	AT2G47260	AT2G47260
LOC115712362	0.93	ARR-B	AT1G67710	response regulator 11
LOC115719254	0.93	TALE	AT2G35940	BEL1-like homeodomain 1 (BLH1)
LOC115707532	0.93	MYB_related	AT3G16350	Homeodomain-like superfamily protein
LOC115699128	0.92	MYB	AT5G49620	AT5G49620
LOC115719098	0.92	C3H	AT5G58620	zinc finger (CCCH-type) family protein
LOC115723142	0.92	GATA	AT3G24050	AT3G24050
LOC115712323	0.92	NAC	AT1G34190	AT1G34190
LOC115718941	0.92	AP2	AT2G28550	related to AP2.7
LOC115708726	0.92	MYB	AT1G49010	Duplicated homeodomain-like superfamily prot.
LOC115705779	0.91	MYB	AT5G04760	Duplicated homeodomain-like superfamily prot.
LOC115713946	0.91	ERF	AT1G78080	related to AP2 4
LOC115697194	0.91	C2H2	AT1G34370	C2H2 and C2HC zinc fingers superfamily protein
LOC115701489	0.91	NAC	AT5G61430	NAC domain containing protein 100
LOC115723252	0.91	NAC	AT3G04070	AT3G04070
LOC115714126	0.91	bZIP	AT5G10030	TGACG motif-binding factor 4
LOC115706074	0.91	HD-ZIP	AT2G46680	homeobox 7
LOC115706266	0.9	NAC	AT4G27410	NAC (No Apical Meristem)
LOC115723418	0.9	MYB	AT3G06490	AT3G06490
LOC115719431	0.9	MYB_related	AT3G46130	myb domain protein 48
LOC115708229	0.9	ERF	AT5G64750	AT5G64750

JA-responsive genes. EIN3 interacts with MYC to modulate these responses, allowing cross-talk between ethylene and JA pathways. This cross-regulation may be crucial for trichome formation and secondary metabolite production. A curated list of TF candidate hubs from the TALE, bHLH, EIL, MYB, and WRKY families is provided in Table S10. For each gene, we provide genomic IDs, best *Arabidopsis* hits, functional descriptions, and transcription factor classifications, along with module assignments and gene expression correlations with cannabinoid and total polyphenol content. This represents a valuable resource for both the scientific community and cannabis breeders, particularly because the data were generated from plants grown in an open-field production pilot, closely reflecting real-world hemp cultivation conditions.

Additionally, another PCA was performed on a subset of 30 samples (inflorescences from DS1 and DS2 at HT2) to include terpene quantifications alongside other metabolites and AA (Fig. 5A). This PCA accounted for 73.9 % of the total variance, with PC1 and PC2 explaining 60 % and 13.9 %, respectively. Again, the production of most metabolites associated with the DS2, particularly in the samples treated with 1 mM and 10 mM MeJA. Interestingly, among the terpenes, aPNN, bPNN also associated with DS2, whereas aHML and bCPN associated with DS1 or DS2 control plants.

To relate RNA-seq transcriptional profiles with a broader range of metabolites, a second WGCNA (WGCNA-30; Table S11) was performed on this 30-sample subset, incorporating TTC, and individual terpenes consistently measured across all samples, alongside cannabinoids and antioxidant activity. The same signed hybrid approach was used to ensure consistency with WGCNA-60. Overall, 16 modules of highly correlated genes were found (Table S11). Importantly, two anti-correlated modules (Darkmagenta and Darkorange) exhibited the strongest positive and negative correlations, respectively, with most individual cannabinoids, TCC, and polyphenols (Fig. 5B). These modules were also the most positively and negatively correlated, respectively, to α-pinene, β-pinene and TTC (Fig. 5B). These findings are in line with and reinforce the biochemical data, which showed a trend of negative correlation between the accumulation of monoterpenes and the content of sesquiterpenes (Table 2). Both classes of terpenes originate from the MVA pathway in the cytosol and the MEP pathway in plastids and can compete for the same precursors (IPP and DMAPP). Our data confirm that an increase in one class can reduce the availability of precursors for the other, leading to a negative correlation in their accumulation. Furthermore, we identify two *(E)-β-ocimene synthase* genes (*LOC115716405* and *LOC115716063*) as likely involved in this process. These two genes are highly associated with aPNN and bPNN accumulation ($r = 0.7$) and negatively correlated with aHML and bCPN ($r = -0.4$) (Tables S9, S11, S12).

Although the correlation values for terpenes were slightly lower than those observed for cannabinoids and TPC, this pattern suggests that the common control identified by the WGCNA analyses places upstream of the entire secondary metabolite production pathway.

Further supporting this, a strong overlap was observed between the Midnightblue module in WGCNA-60 and the Darkmagenta module in the WGCNA-30, as well as between the Red module in WGCNA-60 and the Darkorange one in WGCNA-30 (Table S12). These module pairs shared significant genes highly associated (positively and negatively) with cannabinoids, TPC, AA, α-pinene, β-pinene and TTC (Fig. S5, Table S12), reinforcing the robustness of the identified gene networks in secondary metabolite regulation.

A GCN analysis was performed to explore the regulatory networks underlying the MeJA-induced increase in secondary metabolites at DS2. Genes with MM ≥ 0.8 from the Midnightblue and Red modules of WGCNA-60 were selected, and gene expression values from 60 RNA-seq samples were correlated (Pearson's coefficient $\geq |0.8|$). The GCN structure, visualisation topological and analysis were performed using Cytoscape (Fig. 6). The tight GCN included 2448 genes distributed between the two anticorrelated modules (Fig. 6A). Topological analyses identified key hub genes based on high "Degree" (number of direct

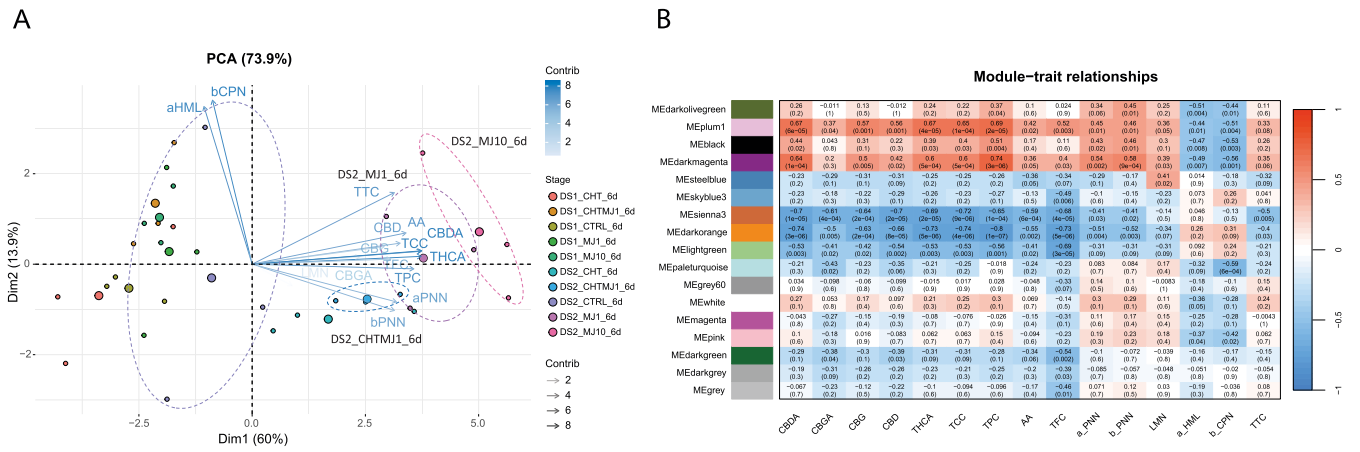

Fig. 5. Principal component analysis of metabolites and WGCNA-30 results. **A)** PCA obtained using all the metabolites from HT2 samples at DS1 and DS2 developmental stages. **B)** Module-trait relationships in WGCNA-30, with module-trait relationships representing the correlation between module eigengenes (MEs) and metabolite content. Each square contains Pearson's correlation coefficient between the MEs and trait (metabolite) and their associated p-values (in brackets underneath). The red and blue colours show a strong positive and negative correlation, respectively. Metabolites: individual (CBDA, CBD, CBGA, CBG, THCA) and total cannabinoids content (TCC), total phenolic content (TPC), antioxidant activity (AA), total flavonoid content (TFC), monoterpenes (aPNN, bPNN, LMN), individual sesquiterpenes (aHML, bCPN) and total terpenes content (TTC).

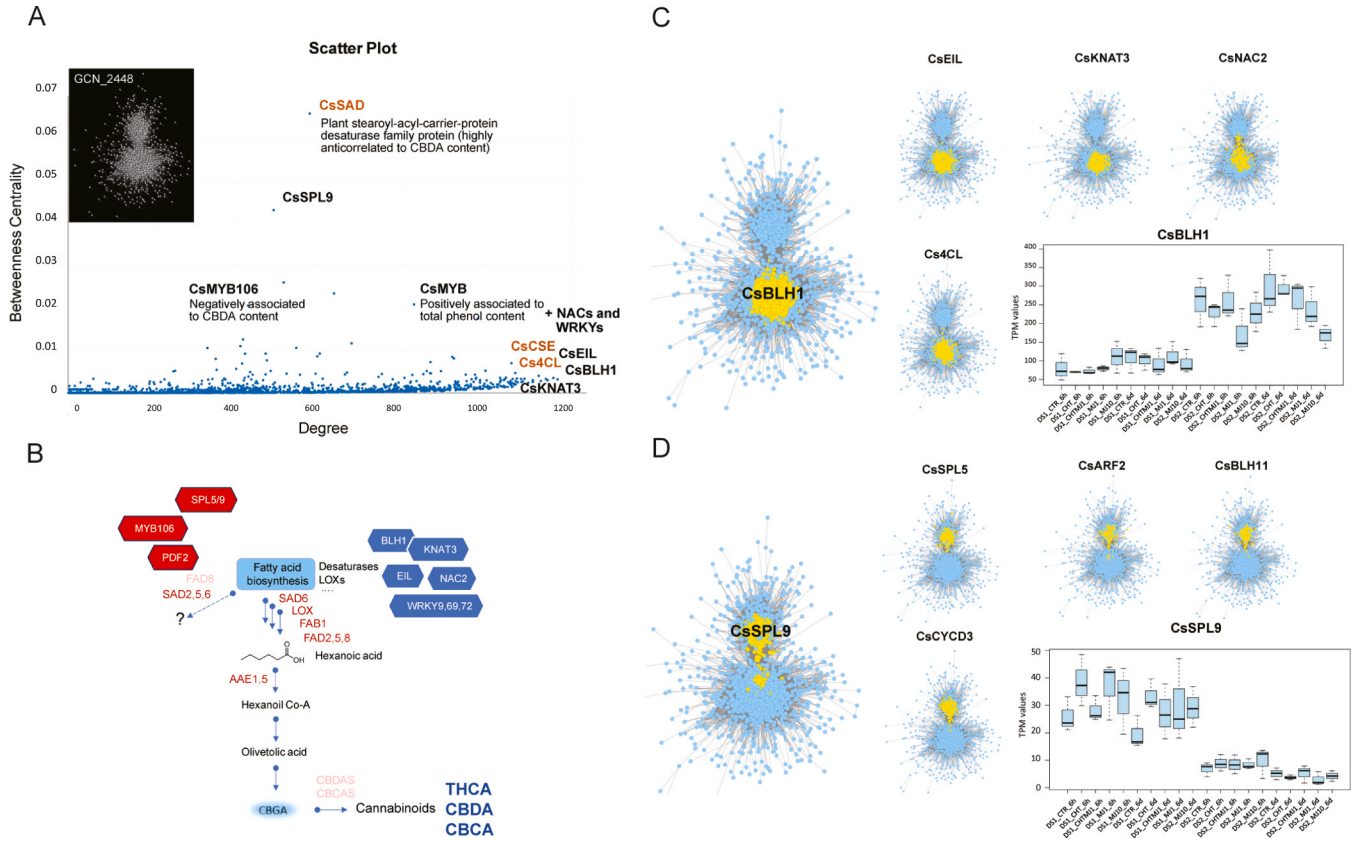

Fig. 6. GCN analysis of the two anticorrelated modules in WGCNA-60 which are strongly positively (Midnightblue) or negatively (Red) associated with secondary metabolites. **A**) Topological analysis of the GCN (image shown at the top left of the scatter plot, with 2448 indicating the number of genes in the GCN), with Degree (number of connections) on the x-axis and Betweenness Centrality on the y-axis. **B**) Main transcription factors (hexagons) positively (blue) or negatively (red) correlated to secondary metabolites. Genes in the fatty acid biosynthetic pathways were identified among the system hubs, with *SAD2,5,6* highly correlated to red TFs (anticorrelated to cannabinoids production), and *SAD6, LOX, FAB1, FAD2,5,8, AAE1,5* correlated to blue TFs (positively associated with cannabinoids production). **C**) Main hubs in the GCN from the Midnightblue module, with nodes connected to the specific hubs highlighted in yellow, and *CsBLH1* gene expression plot in DS1 (first 10 samples on the x-axis) and DS2 (second 10 samples on the x-axis). **D**) Main hubs in the GCN from the Red module, with nodes connected to the specific hubs highlighted in yellow, and *CsSPL9* gene expression plot in DS1 (first 10 samples on the x-axis) and DS2 (second 10 samples on the x-axis). The reliability of the RNA-seq transcriptional profiles was confirmed by RNA-seq data correlation with RT-qPCR results (Fig. S7, Table S14).

connections with other genes) and high "Betweenness centrality" (genes bridging distinct clusters) (Fig. 6A, Table S13). These are two centrality indexes widely used to prioritize genes in a gene co-expression network (Hu et al., 2016). Using only genes with high module membership (MM) within the transcriptional modules identified by WGCNA, and centrality indexes in the GCN, genes with an important regulatory role in the transcriptional network can be predicted. Among TFs, TALE (*BLH1, KNAT3*), EIL, WRKY, and NAC members had the highest degree values and correlated with genes in phenylpropanoid and fatty acid biosynthesis (Fig. 6A-B). Within the phenylpropanoid pathway, two genes emerged as important system hubs, with a high degree in the network and high correlation to *BLH1* (r = 0.96). These genes encode for the caffeoyl shikimate esterase (CSE, *LOC115711963*), a key enzyme in lignin biosynthesis, and the acyl-activating enzyme 4-coumarate–CoA ligase (4CL, *LOC115699132*), which is central to the biosynthesis of both lignin and flavonoids**.** Other acyl-activating enzymes (AAEs) are important hubs in the system that link to the fatty acid pathway (Fig. 6B), most importantly to hexanoic acid and cannabinoids biosynthesis. Given that AAEs activate substrates such as phenylpropanoids, fatty acids, and jasmonate precursors, they may regulate multiple secondary metabolite classes. Several genes with high betweenness centrality were identified, suggesting regulatory roles in secondary metabolite production (e.g. MYBs). The highest betweenness centrality was observed for a gene encoding a stearoyl-acyl-carrier-protein desaturase (CsSAD, *LOC115707488*), a homolog of *Arabidopsis SAD6/FTM1* gene (*AT1G43800*) (Fig. 6A). SAD enzymes regulate C18 unsaturated fatty acid pools, influencing oleic acid homeostasis. *SAD6* (Red module) was a major negative hub in the GCN, anticorrelated with secondary metabolites (e.g. CBDA) accumulation, and strongly correlated (r = 0.96) with a TF (*LOC115698708*) homologous to *Arabidopsis MYB106*, another negative network hub. In *Arabidopsis*, MYB106 inhibits trichome branching and epidermal cell development, suggesting a possible antagonistic role in cannabinoid biosynthesis (Oshima et al., 2013).

Overall, our finding confirmed and strengthened a pivotal role of fatty acids and oleic acid homeostasis as a central and limiting step to produce cannabinoids, rather than downstream cannabinoids biosynthetic genes such as THCAS, CBCAS and CBDAS. Several genes in the fatty acid and hexanoate pathways, which supplies the key cannabinoid precursor, were found among the GCN hubs (Fig. 6B), displayed DS2 stage-specific expression and some were upregulated by the MeJa treatment only at DS2.

Genes homologous to *Arabidopsis BLH1*, *KNAT3* and *EIL* were identified as major hubs associated to secondary metabolite production (Fig. 6C), together with WRKY and NAC TFs**.** Other TALE TFs homologous to *Arabidopsis KNAT7* and *BELL1* also displayed high degree in the network (Table 5). *SQUAMOSA (SPL9, SPL5) HSF, TALE (BLH11)* and *ARF* TFs were associated with the anticorrelated Red module. This subnetwork (Fig. 6D) included cell cycle regulators (*CYCD3, CYCB, CDKB*), supporting the idea that secondary metabolite accumulation is driven by inflorescence maturation and MeJA-induced trichome development, as evidenced in different species (Feng et al., 2021). TALE (KNOX, BELL-like/BLH) TFs play crucial role in meristem maintenance and differentiation (Di Giacomo et al., 2013), with class 2 KNOX genes, such as *KNAT3*, promoting cell differentiation, while class 1 KNOX genes promote meristem maintenance (Di Giacomo et al., 2017; Furumizu et al., 2015). Here, we identified novel roles for hemp *BLH1* and *KNAT3* homologues in promoting cell differentiation associated to secondary metabolites production, antagonistically to *SPL9* and *SPL5* that promote meristematic fate and cell division in hemp inflorescence. In *Arabidopsis*, *SPL9* negatively regulates trichome formation (Yu et al., 2010) and directly controls cell cycle genes (cyclins), essential for cell cycle progression and meristem maintenance.

Markers of functional glandular trichome formation described in Huang et al. (Huang et al., 2024) associated to DS2 samples and were highly co-expressed with *BLH1* and *KNAT3* homologues (Fig. S6), with *CsWRKY69* showing the highest correlation (r = 0.96).

4. Conclusions

In this open-field study, phenols, cannabinoids, terpenes, and antioxidant activity were assessed in Tiborszallasi female inflorescences following several elicitation treatments during flower development. Biochemical and transcriptomic analyses revealed molecular mechanisms underlying secondary metabolite induction. The biochemical results indicated that metabolite accumulation was primarily influenced by developmental stage, harvest time, and MeJA treatment. Notably, 10 mM MeJA had a strong effect, particularly on mature inflorescences. MeJA treatments (MJ1, MJ10) triggered broader transcriptomic changes than chitosan (CHT, CHTMJ1), peaking within 6 h of 10 mM MeJA exposure, regardless of flower developmental stage. The 10 mM MeJA treatment significantly influenced gene transcription for phenolic biosynthesis at DS1 and DS2 and lipid biosynthesis at DS1. Hydroxycinnamic acid and monolignol pathway genes showed a rapid, dose-dependent response, correlating with increased TPC. Conversely, transcriptomic changes in cannabinoid biosynthesis were limited to DS2 after 10 mM MeJA treatment. It is important to note that the observed increase in secondary metabolites refers specifically to the Tiborszallasi variety used in this study. However, while the absolute magnitude of the response may vary across different genotypes, similar elicitor-induced trends in secondary metabolite accumulation have been widely reported, supporting the broader relevance of our findings. Integrated biochemical and transcriptomic analyses revealed common regulatory pathways for cannabinoids, terpenes, and phenolics, involving both known and novel transcription factors and metabolic genes as potential regulatory hubs in secondary metabolite biosynthesis under MeJA treatment. Key regulatory genes belonging to the TALE, EIN and SPL classes of TFs were, for the first time, implicated in the developmental regulatory network underlying glandular trichome formation. This developmental genetic context appears to be key in enabling hemp inflorescences to respond to MeJA-induced elicitation of cannabinoids, through the activation and regulation of fatty acid and hexanoic acid precursor biosynthesis. Additionally, a list of known and novel MYB, NAC, and WRKY TFs associated with the production of secondary metabolites was provided as a valuable resource for the scientific community and breeders. This is especially significant because the data were generated from Tiborszallasi plants grown in an open-field production pilot, closely reflecting real-world cultivation conditions.

CRediT authorship contribution statement

Douguè Kentsop Roméo Arago: Writing – review & editing, Writing – original draft, Visualization, Investigation. **Giulio Testone:** Writing – review & editing, Writing – original draft, Visualization, Investigation, Formal analysis. **Monica Mattana:** Writing – review & editing, Supervision, Project administration, Funding acquisition, Conceptualization. **Annamaria Genga:** Writing – review & editing, Investigation, Conceptualization. **Incoronata Galasso:** Writing – review & editing, Supervision, Investigation. **Cassia da Silva Linge:** Investigation, Formal analysis. **Donato Giannino:** Writing – review & editing, Conceptualization. **Giovanna Frugis:** Writing – review & editing, Writing – original draft, Visualization, Supervision, Investigation, Formal analysis, Conceptualization. **Gabriella Roda:** Investigation. **Stefano Biffani:** Formal analysis. **Andrea Delledonne:** Investigation.

Declaration of Competing Interest

The authors declare the following financial interests/personal relationships which may be considered as potential competing interests: Monica Mattana reports financial support was provided by Lombardy Region. If there are other authors, they declare that they have no known competing financial interests or personal relationships that could have

appeared to influence the work reported in this paper.

Acknowledgments

This research was funded by Regione Lombardia, dds n. 4403 28/03/2018, grant n. 19 - "MITICAL".

Appendix A. Supporting information

Supplementary data associated with this article can be found in the online version at doi:10.1016/j.indcrop.2025.121749.

Data availability

Data will be made available on request.

References

Aizpurua-Olaizola, O., Soydaner, U., Ozturk, E., Schibano, D., Simsir, Y., Navarro, P., Etxebarria, N., Usobiaga, A., 2016. Evolution of the cannabinoid and terpene content during the growth of *cannabis sativa* plants from different chemotypes. J. Nat. Prod. 79, 324–331.

Amaducci, S., Scordia, D., Liu, F.H., Zhang, Q., Guo, H., Testa, G., Cosentino, S.L., 2015. Key cultivation techniques for hemp in Europe and China. Ind. Crops Prod. 68, 2–16.

Andre, C.M., Hausman, J.F., Guerriero, G., 2016. *cannabis sativa*: the plant of the thousand and one molecules. Front Plant Sci. 7, 19.

Apicella, P.V., Sands, L.B., Ma, Y., Berkowitz, G.A., 2022. Delineating genetic regulation of cannabinoid biosynthesis during female flower development in *cannabis sativa*. Plant Direct 6, e412.

Arya, S.S., Rookes, J.E., Cahill, D.M., Lenka, S.K., 2022. Chitosan nanoparticles and their combination with methyl jasmonate for the elicitation of phenolics and flavonoids in plant cell suspension cultures. Int. J. Biol. Macromol. 214, 632–641.

Bahieldin, A., Atef, A., Edris, S., Gadalla, N.O., Al-Matary, M., Al-Kordy, M.A., Ramadan, A.M., Bafeel, S., Alharbi, M.G., Al-Quwaie, D.A.H., Sabir, J.S.M., Al-Zahrani, H.S., Nasr, M.E., El-Domyati, F.M., 2018. Stepwise response of MeJA-induced genes and pathways in leaves of *c. roseus*. Comptes rendus. Biol. 341, 411–420.

Behr, M., Pokorna, E., Dobrev, P.I., Motyka, V., Guignard, C., Lutts, S., Hausman, J.F., Guerriero, G., 2019. Impact of jasmonic acid on lignification in the hemp hypocotyl. Plant Signal Behav. 14, 1592641.

Beleggia, R., Iannucci, A., Menga, V., Quitadamo, F., Suriano, S., Citti, C., Pecchioni, N., Trono, D., 2023. Impact of chitosan-based foliar application on the phytochemical content and the antioxidant activity in hemp (*cannabis sativa* L.) inflorescences. Plants (Basel) 12, 3692.

Bolger, A.M., Lohse, M., Usadel, B., 2014. Trimmomatic: a flexible trimmer for illumina sequence data. Bioinformatics 30, 2114–2120.

Booth, J.K., Yuen, M.M.S., Jancsik, S., Madilao, L.L., Page, J.E., Bohlmann, J., 2020. Terpene synthases and terpene variation in *cannabis sativa*. Plant Physiol. 184, 130–147.

Borrego, E.J., Robertson, M., Taylor, J., Schultzhaus, Z., Espinoza, E.M., 2023. Oxylipin biosynthetic gene families of *cannabis sativa*. PLoS One 18, e0272893.

Cao, X., Yan, J., Lei, J., Li, J., Zhu, J., Zhang, H., 2017. De novo transcriptome sequencing of MeJA-induced taraxacum koksaghyz rodin to identify genes related to rubber formation. Sci. Rep. 7, 15697.

Chen, J., Wang, J., Wang, R., Xian, B., Ren, C., Liu, Q., Wu, Q., Pei, J., 2020. Integrated metabolomics and transcriptome analysis on flavonoid biosynthesis in safflower (*carthamus tinctorius* L.) under MeJA treatment. BMC Plant Biol. 20, 353.

Conneely, L.J., Hurgobin, B., Ng, S., Tamiru-Oli, M., Lewsey, M.G., 2024. Characterization of the *Cannabis sativa* glandular trichome epigenome. bioRxiv, 2024.2007.2004.602151.

Dei Cas, M., Casagni, E., Casiraghi, A., Minghetti, P., Fornasari, D.M.M., Ferri, F., Arnoldi, S., Gambaro, V., Roda, G., 2020. Phytocannabinoids profile in medicinal *cannabis* oils: the impact of plant varieties and preparation methods. Front. Pharmacol. 11, 570616.

Dei Cas, M., Arnoldi, S., Monguzzi, L., Casagni, E., Morano, C., Vieira de Manincor, E., Bolchi, C., Pallavicini, M., Gambaro, V., Roda, G., 2021. Characterization of chemotype-dependent terpenoids profile in cannabis by headspace gas-chromatography coupled to time-of-flight mass spectrometry. J. Pharm. Biomed. Anal. 203, 114180.

Di Giacomo, E., Iannelli, M.A., Frugis, G., 2013. TALE and shape: how to make a leaf different. Plants (Basel) 2, 317–342.

Di Giacomo, E., Laffont, C., Sciarra, F., Iannelli, M.A., Frugier, F., Frugis, G., 2017. *knat3/4/5*-like class 2 KNOX transcription factors are involved in *medicago truncatula* symbiotic nodule organ development. New Phytol. 213, 822–837.

Duhan, J.S., Kumar, R., Kumar, N., Kaur, P., Nehra, K., Duhan, S., 2017. Nanotechnology: the new perspective in precision agriculture. Biotechnol. Rep. (Amst.) 15, 11–23.

Fäldt, J., Arimura, G.-i, Gershenzon, J., Takabayashi, J., Bohlmann, J., 2003. Functional identification of *attps03* as (*e*)-β-ocimene synthase: a monoterpene synthase catalyzing jasmonate- and wound-induced volatile formation in *arabidopsis thaliana*. Planta 216, 745–751.

Fayaz, M., Kundan, M., Gani, U., Sharma, P., Wajid, M.A., Katoch, K., Babu, V., Gairola, S., Misra, P., 2023. Identification of lipoxygenase gene repertoire of *cannabis sativa* and functional characterization of *cslox13* gene. Plant Sci. 334, 111780.

Feng, Z., Bartholomew, E.S., Liu, Z., Cui, Y., Dong, Y., Li, S., Wu, H., Ren, H., Liu, X., 2021. Glandular trichomes: new focus on horticultural crops. Hortic. Res. 8, 158.

Furumizu, C., Alvarez, J.P., Sakakibara, K., Bowman, J.L., 2015. Antagonistic roles for KNOX1 and KNOX2 genes in patterning the land plant body plan following an ancient gene duplication. PLoS Genet. 11, e1004980.

Gabotti, D., Locatelli, F., Cusano, E., Baldoni, E., Genga, A., Pucci, L., Consonni, R., Mattana, M., 2019. Cell suspensions of *cannabis sativa* (var. Futura): effect of elicitation on metabolite content and antioxidant activity. Molecules 24, 4056.

Garrido, J., Rico, S., Corral, C., Sanchez, C., Vidal, N., Martinez-Quesada, J.J., Ferreiro-Vera, C., 2022. Exogenous application of stress-related signaling molecules affect growth and cannabinoid accumulation in medical cannabis (*cannabis sativa* L.). Front. Plant Sci. 13, 1082554.

GlobeNewswire, 2025. Hemp-derived Cannabidiol Market Report 2025: Growing Demand for CBD in Personal Care and Cosmetics, Regulatory Changes and Shift Toward Natural and Plant-based Wellness Products, Dublin, Ireland.

Graña, E., Díaz-Tielas, C., Sánchez-Moreiras, A.M., Reigosa, M.J., Celeiro, M., Abagyan, R., Teijeira, M., Duke, M.V., Clerk, T., Pan, Z., Duke, S.O., 2020. Transcriptome and binding data indicate that citral inhibits single strand DNA-binding proteins. Physiol. Plant 169, 99–109.

Hickman, R., Van Verk, M.C., Van Dijken, A.J.H., Mendes, M.P., Vroegop-Vos, I.A., Caarls, L., Steenbergen, M., Van der Nagel, I., Wesselink, G.J., Jironkin, A., Talbot, A., Rhodes, J., De Vries, M., Schuurink, R.C., Denby, K., Pieterse, C.M.J., Van Wees, S.C.M., 2017. Architecture and dynamics of the jasmonic acid gene regulatory network. Plant Cell 29, 2086–2105.

Hu, J.X., Thomas, C.E., Brunak, S., 2016. Network biology concepts in complex disease comorbidities. Nat. Rev. Genet. 17, 615–629.

Huang, X., Chen, W., Zhao, Y., Chen, J., Ouyang, Y., Li, M., Gu, Y., Wu, Q., Cai, S., Guo, F., Zhu, P., Ao, D., You, S., Vasseur, L., Liu, Y., 2024. Deep learning-based quantification and transcriptomic profiling reveal a methyl jasmonate-mediated glandular trichome formation pathway in *cannabis sativa*. Plant J. 118, 1155–1173.

Humbal, A., Pathak, B., 2023. Harnessing nanoparticle-mediated elicitation in plant tissue culture: a promising approach for secondary metabolite production. Plant Cell Tissue Organ Cult. 155, 385–402.

Izzo, L., Castaldo, L., Narvaez, A., Graziani, G., Gaspari, A., Rodriguez-Carrasco, Y., Ritieni, A., 2020. Analysis of phenolic compounds in commercial *cannabis sativa* L. Inflorescences using UHPLC-Q-orbitrap HRMS. Molecules 25, 631.

Jadoon, L., Gul, A., Fatima, H., Babar, M.M., 2024. Nano-elicitation and hydroponics: a synergism to enhance plant productivity and secondary metabolism. Planta 259, 80.

Kim, D., Paggi, J.M., Park, C., Bennett, C., Salzberg, S.L., 2019. Graph-based genome alignment and genotyping with HISAT2 and HISAT-genotype. Nat. Biotechnol. 37, 907–915.

Kobtrakul, K., Rani, D., Binalee, A., Udomlarp, P., Srichai, T., De-Eknamkul, W., Vimolmangkang, S., 2023. Elicitation enhances the production of friedelin and epifriedelanol in hairy root cultures of *cannabis sativa* l. Front. Plant Sci. 14, 1242584.

Langfelder, P., Horvath, S., 2008. WGCNA: an r package for weighted correlation network analysis. BMC Bioinforma. 9, 559.

Liu, R., Niimi, H., Ueda, M., Takaoka, Y., 2022. Coordinately regulated transcription factors EIN3/EIL1 and MYCs in ethylene and jasmonate signaling interact with the same domain of MED25. Biosci. Biotechnol. Biochem. 86, 1405–1412.

Liu, S., Fu, Y., He, Y., Zeng, X., 2021. Transcriptome analysis of the impact of exogenous methyl jasmonate on the opening of sorghum florets. PLoS One 16, e0248962.

Liu, Z., Zhu, X., Mohsin, A., Sun, H., Du, L., Yin, Z., Zhuang, Y., Guo, M., 2024. Uncovering the role of hydroxycinnamoyl transferase in boosting chlorogenic acid accumulation in *carthamus tinctorius* cells under methyl jasmonate elicitation. Int. J. Mol. Sci. 25, 2710.

Livingston, S.J., Quilichini, T.D., Booth, J.K., Wong, D.C.J., Rensing, K.H., Laflamme-Yonkman, J., Castellarin, S.D., Bohlmann, J., Page, J.E., Samuels, A.L., 2020. Cannabis glandular trichomes alter morphology and metabolite content during flower maturation. Plant J. 101, 37–56.

Love, M.I., Huber, W., Anders, S., 2014. Moderated estimation of fold change and dispersion for RNA-seq data with DESeq2. Genome Biol. 15, 550.

Lowe, H., Steele, B., Bryant, J., Toyang, N., Ngwa, W., 2021. Non-cannabinoid metabolites of *cannabis sativa* L. With therapeutic potential. Plants (Basel) 10, 400.

Mandolino, G., Carboni, A., Forapani, S., Faeti, V., Ranalli, P., 1999. Identification of DNA markers linked to the Male sex in dioecious hemp (*cannabis sativa* L.). Theor. Appl. Genet. 98, 86–92.

Martínez-Chávez, L.A., Hernández-Ramírez, M.Y., Feregrino-Pérez, A.A., Esquivel Escalante, K., 2024. Cutting-edge strategies to enhance bioactive compound production in plants: potential value of integration of elicitation, metabolic engineering, and Green nanotechnology. Agron. (Basel) 14, 2822.

Matthes, M.C., Pickett, J.A., Napier, J.A., 2008. Natural variation in responsiveness of *arabidopsis thaliana* to methyl jasmonate is developmentally regulated. Planta 228, 1021–1028.

Mirzamohammad, E., Alirezalu, A., Alirezalu, K., Norozi, A., Ansari, A., 2021. Improvement of the antioxidant activity, phytochemicals, and cannabinoid compounds of *cannabis sativa* by salicylic acid elicitor. Food Sci. Nutr. 9, 6873–6881.

Mishchenko, S., Mokher, J., Laiko, I., Burbulis, N., Kyrychenko, H., Dudukova, S., 2017. Phenological growth stages of hemp (*cannabis sativa* L.): codification and description according to the BBCH scale. ŽemėS. ūkio Moksl. 24, 31–36.

Mmereke, K.M., Venkataraman, S., Moiketsi, B.N., Khan, M.R., Hassan, S.H., Rantong, G., Masisi, K., Kwape, T.E., Gaobotse, G., Zulfiqar, F., Kumar Sharma, S., Malik, S.,

Makhzoum, A., 2024. Nanoparticle elicitation: a promising strategy to modulate the production of bioactive compounds in hairy roots. Food Res. Int. 178, 113910.
Mukherjee, K., Brocchieri, L., Burglin, T.R., 2009. A comprehensive classification and evolutionary analysis of plant homeobox genes. Mol. Biol. Evol. 26, 2775–2794.
Oshima, Y., Shikata, M., Koyama, T., Ohtsubo, N., Mitsuda, N., Ohme-Takagi, M., 2013. MIXTA-Like transcription factors and WAX INDUCER1/SHINE1 coordinately regulate cuticle development in arabidopsis and *torenia fournieri*. Plant Cell 25, 1609–1624.
Pancaldi, F., Salentijn, E.M.J., Trindade, L.M., 2025. From fibers to flowering to metabolites: unlocking hemp (*cannabis sativa*) potential with the guidance of novel discoveries and tools. J. Exp. Bot. 76, 109–123.
Pauwels, L., Morreel, K., De Witte, E., Lammertyn, F., Van Montagu, M., Boerjan, W., Inze, D., Goossens, A., 2008. Mapping methyl jasmonate-mediated transcriptional reprogramming of metabolism and cell cycle progression in cultured arabidopsis cells. Proc. Natl. Acad. Sci. USA 105, 1380–1385.
Pękal, A., Pyrzynska, K., 2014. Evaluation of aluminium complexation reaction for flavonoid content assay. Food Anal. Methods 7, 1776–1782.
Pertea, M., Pertea, G.M., Antonescu, C.M., Chang, T.C., Mendell, J.T., Salzberg, S.L., 2015. StringTie enables improved reconstruction of a transcriptome from RNA-seq reads. Nat. Biotechnol. 33, 290–295.
Picchi, V., Calzone, A., Gobbi, S., Paccani, S., Lo Scalzo, R., Marti, A., Faoro, F., 2022. Oxidative stress mitigation by chitosan nanoparticles in durum wheat also affects phytochemicals and technological quality of bran and semolina. Plants (Basel) 11, 2021.
Qin, W., Yin, Q., Chen, J., Zhao, X., Yue, F., He, J., Yang, L., Liu, L., Zeng, Q., Lu, F., Mitsuda, N., Ohme-Takagi, M., Wu, A.M., 2020. The class II KNOX transcription factors *knat3* and *knat7* synergistically regulate monolignol biosynthesis in arabidopsis. J. Exp. Bot. 71, 5469–5483.
Russo, E.B., Jiang, H.-E., Li, X., Sutton, A., Carboni, A., del Bianco, F., Mandolino, G., Potter, D.J., Zhao, Y.-X., Bera, S., Zhang, Y.-B., Lü, E.-G., Ferguson, D.K., Hueber, F., Zhao, L.-C., Liu, C.-J., Wang, Y.-F., Li, C.-S., 2008. Phytochemical and genetic analyses of ancient cannabis from Central Asia. J. Exp. Bot. 59, 4171–4182.
Schmelz, S., Naismith, J.H., 2009. Adenylate-forming enzymes. Curr. Opin. Struct. Biol. 19, 666–671.
Seo, H.S., Song, J.T., Cheong, J.J., Lee, Y.H., Lee, Y.W., Hwang, I., Lee, J.S., Choi, Y.D., 2001. Jasmonic acid carboxyl methyltransferase: a key enzyme for jasmonate-regulated plant responses. Proc. Natl. Acad. Sci. USA 98, 4788–4793.
Shannon, P., Markiel, A., Ozier, O., Baliga, N.S., Wang, J.T., Ramage, D., Amin, N., Schwikowski, B., Ideker, T., 2003. Cytoscape: a software environment for integrated models of biomolecular interaction networks. Genome Res. 13, 2498–2504.
Shi, J., Ma, C., Qi, D., Lv, H., Yang, T., Peng, Q., Chen, Z., Lin, Z., 2015. Transcriptional responses and flavor volatiles biosynthesis in methyl jasmonate-treated tea leaves. BMC Plant Biol. 15, 233.
Sirangelo, T.M., Ludlow, R.A., Spadafora, N.D., 2022. Multi-omics approaches to study molecular mechanisms in *cannabis sativa*. Plants (Basel) 11, 2182.
Stout, J.M., Boubakir, Z., Ambrose, S.J., Purves, R.W., Page, J.E., 2012. The hexanoyl-CoA precursor for cannabinoid biosynthesis is formed by an acyl-activating enzyme in *cannabis sativa* trichomes. Plant J. 71, 353–365.
Thakur, M., Bhattacharya, S., Khosla, P.K., Puri, S., 2019. Improving production of plant secondary metabolites through biotic and abiotic elicitation. J. Appl. Res. Med. Aroma Plants 12, 1–12.
The Business Research Company, 2024. Hemp global market report 2025.
Trono, D., 2024. Elicitation as a tool to improve the accumulation of secondary metabolites in *cannabis sativa*. Phytochem. Rev.
Wang, B., Niu, J., Li, B., Huang, Y., Han, L., Liu, Y., Zhou, W., Hu, S., Li, L., Wang, D., Wang, S., Cao, X., Wang, Z., 2018. Molecular characterization and overexpression of *smjmt* increases the production of phenolic acids in *salvia miltiorrhiza*. Int. J. Mol. Sci. 19, 3788.
Wang, J., Cui, Y., Li, S., Gao, X., Zhang, K., Shen, X., 2023. Transcriptome analysis of *artemisia argyi* following methyl jasmonate (MeJA) treatment and the mining of genes related to the stress resistance pathway. Front. Genet. 14, 1279850.
Wei, S., 2010. Methyl jasmonic acid induced expression pattern of terpenoid indole alkaloid pathway genes in *catharanthus roseus* seedlings. Plant Growth Regul. 61, 243–251.
Welling, M.T., Deseo, M.A., O'Brien, M., Clifton, J., Bacic, A., Doblin, M.S., 2023. Metabolomic analysis of methyl jasmonate treatment on phytocannabinoid production in *cannabis sativa*. Front. Plant Sci. 14, 1110144.
Wu, T., Hu, E., Xu, S., Chen, M., Guo, P., Dai, Z., Feng, T., Zhou, L., Tang, W., Zhan, L., Fu, X., Liu, S., Bo, X., Yu, G., 2021. Clusterprofiler 4.0: a universal enrichment tool for interpreting omics data. Innov. (Camb.) 2, 100141.
Yang, R., Berthold, E.C., McCurdy, C.R., da Silva Benevenute, S., Brym, Z.T., Freeman, J. H., 2020. Development of cannabinoids in flowers of industrial hemp (*cannabis sativa* L.): a pilot study. J. Agric. Food Chem. 68, 6058–6064.
Yao, D., Zhang, Z., Chen, Y., Lin, Y., Xu, X., Lai, Z., 2021. Transcriptome analysis reveals differentially expressed genes that regulate biosynthesis of the active compounds with methyl jasmonate in rosemary suspension cells. Genes 13, 67.
Yu, N., Cai, W.J., Wang, S., Shan, C.M., Wang, L.J., Chen, X.Y., 2010. Temporal control of trichome distribution by microRNA156-targeted SPL genes in arabidopsis thaliana. Plant Cell 22, 2322–2335.
Zhu, J., Chen, H., Liu, L., Xia, X., Yan, X., Mi, X., Liu, S., Wei, C., 2024. JA-mediated MYC2/LOX/AOS feedback loop regulates osmotic stress response in tea plant. Hortic. Plant J. 10, 931–946.
Zulak, K.G., Lippert, D.N., Kuzyk, M.A., Domanski, D., Chou, T., Borchers, C.H., Bohlmann, J., 2009. Targeted proteomics using selected reaction monitoring reveals the induction of specific terpene synthases in a multi-level study of methyl jasmonate-treated Norway spruce (*picea abies*). Plant J. 60, 1015–1030.